A&A, 687, A132 (2024)
https://doi.org/10.1051/0004-6361/202347616

Astronomy & Astrophysics

Joint analysis of JUICE and Europa Clipper tracking data to study the Jovian system ephemerides and dissipative parameters

Andrea Magnanini[1], Marco Zannoni[1,2], Luis Gomez Casajus[2], Paolo Tortora[1,2], Valery Lainey[3], Erwan Mazarico[4], Ryan S. Park[5], and Luciano Iess[6]

[1] Dipartimento di Ingegneria Industriale, Alma Mater Studiorum – Università di Bologna, 47121 Forlì (FC), Italy
e-mail: andrea.magnanini3@unibo.it
[2] Centro Interdipartimentale di Ricerca Industriale Aerospaziale, Alma Mater Studiorum – Università di Bologna, 47121 Forlì (FC), Italy
[3] IMCCE, Observatoire de Paris, PSL Research University, CNRS, Sorbonne Université, Université de Lille 1, Paris, France
[4] NASA Goddard Space Flight Center, Greenbelt, MD 20771, USA
[5] Jet Propulsion Laboratory, California Institute of Technology, Pasadena, CA, USA
[6] Department of Mechanical and Aerospace Engineering, Sapienza University of Rome, Via Eudossiana 18, Rome, Italy

Received 31 July 2023 / Accepted 4 March 2024

ABSTRACT

Context. Jupiter and its moons form a complex dynamical system that includes several coupling dynamics at different frequencies. In particular, the Laplace resonance is fundamental to maintaining the energy dissipation that sustain Io's volcanic activity and Europa's subsurface ocean; studying its stability is thus crucial for characterizing the potential habitability of these moons. The origin and evolution of the Laplace resonance is driven by the strong tidal interactions between Jupiter and its Galilean moons, and the future planetary exploration missions JUICE and Europa Clipper could bring new light to this unsolved mechanism. During the Jupiter tours of both missions and JUICE's Ganymede orbital phase, two-way radiometric range and Doppler data will be acquired between Earth ground stations and the spacecraft, which will be processed to recover the static and time-varying gravity field of the moons. Moreover, range and Doppler data will improve the orbit accuracy of the moons, providing precise measurements of Jupiter's tidal parameters.
Aims. This work presents a covariance analysis of the joint orbit determination of JUICE and Europa Clipper, aimed at quantifying the expected uncertainties on the main parameters that characterize the dynamics of the Jupiter system.
Methods. We simulated radio science data from JUICE and Clipper missions under conservative noise assumptions, using a multi-arc approach to estimate the ephemerides and dissipation in the system.
Results. Even though JUICE and Europa Clipper will not perform flybys of Io, the strong coupling with Europa and Ganymede will allow an improvement of our knowledge of the Jupiter-Io dissipation parameters thanks to JUICE and Europa Clipper radiometric data. Moreover, the expected uncertainty in Jupiter's dissipation at the frequency of Callisto could unveil a potential resonance locking mechanism between Jupiter and Callisto.

Key words. methods: data analysis – space vehicles – space vehicles: instruments – ephemerides – planets and satellites: dynamical evolution and stability – planets and satellites: individual: Galilean moons

1. Introduction

The dynamics of Jupiter's Galilean moons, namely Io, Europa, Ganymede, and Callisto, is one of the most intriguing in the Solar System. This is mainly due to the presence of the Laplace resonance between the three innermost moons, which can be expressed as

$$n_1 - 3n_2 + 2n_3 = 0, \quad (1)$$
$$\lambda_1 - 3\lambda_2 + 2\lambda_3 \approx \pi, \quad (2)$$

where n represents the mean motion and λ represents the mean longitude of the moons, while subscripts 1, 2, and 3 denote Io, Europa, and Ganymede, respectively. The first relation is exact in average, while the second oscillates closely around π (Murray & Dermott 1999; Lieske 1998). These relations imply that Io and Europa are in conjunction with respect to Jupiter at Io's perijove and Europa's apojove, respectively, and that there cannot be a triple conjunction.

The most important phenomenon affecting the formation and evolution of a resonance is the tidal dissipation, as first pointed out by Goldreich & Sciama (1965) and successively investigated and confirmed by many other authors and works (Lainey et al. 2017, 2020; Lari et al. 2020). The dissipative phenomena inside Jupiter and its moons have been suggested to be the primary reason the Laplace resonance has formed, as they cause the orbital migration of the moons, making it possible for the orbits to enter into different orbital ratios over time, eventually creating a resonance. However, the origin and the evolution of this resonance is still unclear, mainly due to the lack of precise data. Numerous hypotheses have been proposed. For example, regarding the origin, Yoder & Peale (1981) proposed two potential scenarios. The first assumes that the migration of Io was always faster than the other Galilean moons. This would have resulted in Io capturing Europa into a mean-motion resonance, causing an acceleration in its migration and eventually resulting in the capture of Ganymede into a three-body resonance. The other scenario hypothesized that the resonance arose during the formation

of the Galilean satellites and now it is slowly deteriorating due to tidal dissipation (Lee & Peale 2002).

Alternatively, Malhotra (1991) suggested that the current resonance has been reached through multiple chaotic phases and that many resonances have been crossed. After a resonance is reached, the strongest tidal migration (usually that of the body closest to the central planet) is spread to all the moons in resonance, accelerating their orbital evolution (Yoder & Peale 1981). For the Jovian system, the tidal dissipation between Jupiter and Io is the main source of drifting force and it dominates the Laplace resonance evolution (Lainey et al. 2009; Lari et al. 2020). The same mechanism could also cause the end of the currently existing resonance (Lainey et al. 2009; Lari et al. 2020).

The tidal effects arise when an external perturbing body interacts gravitationally with an extended body. The gradient of the external gravitational field creates a differential gravitational attraction on the different parts of the body, causing a physical deformation with mass redistribution and change in its gravitational field. In the classical model, under the hypothesis of small deformations, the change of the gravity potential coefficients is modeled as linearly proportional to the external tidal field, where the proportionality factor is the Love number k, as shown in Sect. 3. The largest tidal distortion is parallel to the equatorial plane, and the mass redistribution inside the body in response to the forcing potential is mainly expressed by the degree-2 Love number k_2. The actual body's response to the tidal potential depends on the interior structure, such that it can be used to infer the presence and density of a subsurface ocean on icy satellites (Park et al. 2011, 2015; Iess et al. 2012; Mitri et al. 2014).

Assuming a perfect elastic body, the tidal bulge points in the direction of the perturber. However, due to the anelasticity of the body's interior, the tidal bulge is not aligned with the perturber's direction, but lags by some angle, which is called tidal lag, and depends on the amount of friction in the body. Therefore, the k(k_2) can be written as a complex number:

$$k_2 = \mathrm{Re}(k_2) + i\mathrm{Im}(k_2) = |k_2|\,(\cos(\varphi) + i\sin(\varphi)), \tag{3}$$

where the real part of the Love number $Re(k_2)$ expresses the elastic response of the tide body due to the perturber, while the imaginary part of the Love number Im(k_2) reflects the effect of the anelasticity of the body. For small angles, φ is equal to twice the geometrical lag angle between the tide-raising body and the tidal bulge (Efroimsky & Lainey 2007). The phase lag angle φ is related to a widely used parameter in celestial mechanics, called the "quality factor", which is defined as

$$Q = \sin(\varphi)^{-1}. \tag{4}$$

For the tides in a central body raised by a satellite, Q is related to the Love number k_2 as

$$\frac{|k_2|}{Q} = -\mathrm{Im}(k_2). \tag{5}$$

For the tides in a satellite raised by the central body, the equation loses the minus sign. The quality factor Q measures how quickly the body loses energy over time because of dissipative mechanisms, such as friction due to tidal distortion in the body's interior. In analogy with the harmonic oscillator, Q is the ratio of the body's total energy to the energy dissipated per oscillation (tidal frequency) multiplied by 2π. A large quality factor indicates that the object is losing energy very slowly, whereas a small quality factor indicates that the object is losing energy quickly.

Tidal dissipation is the source of energy that sustains the intense volcanic activity on Io and subsurface liquid water oceans inside icy moons, such as Europa, Enceladus, Titan, and possibly Ganymede and Triton (Cassen et al. 1979; Tobie et al. 2005). In general, the dissipation inside these bodies depends on the frequency of the external forcing, as explained in Efroimsky & Lainey (2007) and Efroimsky & Makarov (2013). For a central body with a perturbing satellite, the forcing frequency can be expressed as

$$\chi = 2\left|n - \omega_\mathrm{p}\right|, \tag{6}$$

where n is the mean motion of the satellite orbiting the primary, and ω_p is the spin rotation of the primary.

Tides produce a time variation of the gravity field for both the central planet and its satellites, producing a secular effect on the orbit of the satellite, which, for the dissipative part of the tides, is quadratic with time in tangential direction, and is larger for smaller Q values.

The variation of the semi-major axis and the eccentricity of a satellite due to the tidal dissipation in both the satellite and the primary can be described by the following expressions (Kaula 1964; Peale & Cassen 1978):

$$\frac{\mathrm{d}a}{\mathrm{d}t} = +3\left(\frac{k_2}{Q}\right)_\mathrm{p}\frac{m}{m_\mathrm{p}}\left(\frac{R_\mathrm{p}}{a}\right)^5 na - 21\left(\frac{k_2}{Q}\right)\frac{m_\mathrm{p}}{m}\left(\frac{R}{a}\right)^5 nae^2, \tag{7}$$

$$\frac{\mathrm{d}e}{\mathrm{d}t} = +\frac{57}{8}\left(\frac{k_2}{Q}\right)_\mathrm{p}\frac{m}{m_\mathrm{p}}\left(\frac{R_\mathrm{p}}{a}\right)^5 ne - \frac{21}{2}\left(\frac{k_2}{Q}\right)\frac{m_\mathrm{p}}{m}\left(\frac{R}{a}\right)^5 ne, \tag{8}$$

where the subscript p refers to the planet. The ratio $\left(\frac{k_2}{Q}\right)_\mathrm{p}$ refers to the dissipative parameter of Jupiter at the orbital frequency of the satellite, and n, e, and a refer to its mean motion, eccentricity, and semimajor axis, respectively.

From Eqs. (7)–(8), it can be noticed that the dissipations in the moons tend to circularize the orbit and reduce the semimajor axis, while the dissipation in Jupiter tends to increase the eccentricity and increase the semimajor axis. However, in the case of the Galilean moons, the Laplace resonance forces the eccentricity of the satellites to a nonzero value, keeping their dissipation active (Malhotra 1991; Lari et al. 2023). Characterizing the tidal dissipation in Jupiter and its moons can help to constrain the evolutionary history of the orbits of the moons, which has implications for the assessment of their habitability.

For example, if the Galilean moons were locked in the Laplace resonance early in the history of the Jupiter system, then their subsurface liquid oceans may have existed for a long period of time, perhaps sufficiently long to develop suitable life conditions.

Moreover, Fuller et al. (2016), following the work of Witte & Savonije (1999), also showed that the internal dynamic of the central planet may play a key role in the satellite evolution of gas giant systems. The dynamics of the satellites could enter into resonance with the internal modes of Jupiter, such as inertial waves. This phenomenon, called resonance locking, would contribute to decreasing Jupiter's Q value and would cause a faster tidal migration of satellites with respect to the expectation from classical tidal theory, as observed for the first time for Titan by Lainey et al. (2020).

Regarding the future of the Laplace resonance, Musotto et al. (2002) demonstrated its stability for at least 100 000 yr, while over a timescale of billions of years, Lari et al. (2020) showed how – after an initial inward migration of Io – the moons' configuration is predicted to evolve outward, eventually capturing Callisto in resonance as well. This analysis adopted the dissipation parameters estimated by Lainey et al. (2009), who based their estimations on almost 120 yr of astrometric observables. However, long-term predictions strongly rely on the accuracy of the dissipation parameters, as small changes in their values can completely change the future evolution of the system. Moreover, Lainey et al. (2009) assumed a constant quality factor Q for all the forcing frequencies of the Galilean moons and a frequency-dependent result could also change the long-time evolution of the Laplace resonance.

Hence, studying the orbits of the satellites of Jupiter is crucial in order to characterize the dissipation of the system and constrain the past and future evolution of the Laplace resonance. In addition to Earth-based astrometry, an important tool for inferring precise information about the ephemerides of the Jupiter moons are spacecraft radio science investigations, such as those of Galileo, Juno, JUpiter Icy Moons Explorer (JUICE), and Europa Clipper. In general, spacecraft radio tracking measurements provide better sensitivity to the states of the moons compared to classical astrometry, but they offer limited coverage, as they are only available during the time span of the missions (Fayolle et al. 2023).

Dirkx et al. (2017) studied the observability of the ephemerides and dissipative parameters through JUICE radio tracking data, finding that Jupiter's internal dissipation cannot be clearly estimated with radio science data only. However, these latter authors adopted a simplified approach, not solving for the spacecraft orbit, and therefore effectively not considering the coupling with the ephemerides estimation. Subsequently, Lari & Milani (2019) followed a more complete approach, solving for spacecraft and ephemerides simultaneously. These authors found that the formal uncertainties of the dissipative parameters of Jupiter and Io are expected to be on the same order as those published so far (Lainey et al. 2009). Several other works analyzed the capabilities of radio science investigations of the JUICE and Europa Clipper missions alone, with a focus on gravity-field estimations for Europa, Ganymede, and Callisto, and adopting a simplified approach for the study of the ephemerides, in particular neglecting the tidal dissipation effects on Jupiter (Cappuccio et al. 2020a, 2022; De Marchi et al. 2022; Mazarico et al. 2023). In the present study, we focus on the contribution that both the future missions JUICE and Europa Clipper could bring to the characterization of the ephemerides of the Jupiter system, with a focus on the dissipation parameters, through a joint analysis of expected radiometric data. Our work expands previous analyses on mainly three aspects. First, we aim to combine JUICE and Europa Clipper data. Second, we consider a more realistic set of parameters to be considered in the orbit determination of the probes, including a complete gravity analysis of Europa, Ganymede, and Callisto in order to better assess the expected uncertainty on the spacecraft state and the ephemerides of the moons. Finally, we aim to evaluate, for the first time, the expected uncertainty on the dissipation parameters of Jupiter. To this end, we use a frequency-dependent model, which is considered the most realistic approach by Fuller et al. (2016) and by other authors who analyzed recent observations of the Saturn system (Lainey et al. 2017, 2020). Recently, Fayolle et al. (2023) expanded the analysis described in this manuscript, focusing on possible synergies between spacecraft radio tracking and astrometry data, considering only a constant Q analysis for Jupiter's tides. This paper is organized as follows: Sect. 2 introduces the JUICE and Europa Clipper missions. Section 3 describes the dynamical model for the spacecraft and the Galilean moons. In Sect. 3, we explain the details of the numerical simulations performed, such as the estimation filter setup and the measurement assumptions for JUICE and Europa Clipper spacecraft. The analysis results are discussed in Sect. 5, with a focus on the gravity and tides of Jupiter and the Galilean moons. Finally, in Sect. 6 we summarize our findings.

2. JUICE and Europa Clipper missions

ESA's JUICE and NASA's Europa Clipper are the next two space missions dedicated to the study of the Jupiter system, with a focus on three of the Galilean moons, namely Europa, Ganymede, and Callisto. JUICE (Grasset et al. 2013) was launched in April 2023 and will be inserted in orbit around Jupiter in mid-2031. It will spend 4 yr in the Jovian system and after tens of flybys of Europa, Ganymede, and Callisto, it will enter into orbit around Ganymede, where it will remain for 9 months until end-of-mission. Europa Clipper (Howell & Pappalardo 2020) is currently planned for launch in 2024 and will reach Jupiter in early 2031. It will spend about 4 yr in orbit around Jupiter, performing more than 50 flybys of Europa, the main mission target, and several flybys of Ganymede and Callisto. JUICE is equipped with ten scientific instruments, including the radio science experiment, named Gravity and Geophysics of Jupiter and the Galilean Moons (3GM). This latter is focused on scientific objectives related to gravity, geophysics, and atmospheric science, exploiting the radio link between the spacecraft and the Earth.

An onboard ultra stable oscillator (USO) will be used to perform accurate one-way occultation experiments to study the atmospheres and ionospheres of Jupiter and its satellites. Gravity experiments instead will rely on two-way range and Doppler (range rate) measurements between the spacecraft and a ground station taken by the onboard Ka-band transponder (KaT; Iess & Boscagli 2001), which enables, together with the standard telecommunication transponder, a coherent two-way triple link at X and Ka bands with full plasma noise cancelation for both Doppler and range measurements. During each close encounter, a steerable medium-gain antenna (MGA) will guarantee a radio link, while the 2.5 m high-gain antenna (HGA) will be exploited far from the flybys and during the Ganymede orbital phase. The accuracy of the range and range rate measurements will be similar to those obtained by the MORE investigation on BepiColombo (4 cm and 0.012 mm s^{-1}, respectively at 4.2 s and 60 s integration times) as it benefits from an identical radio system (Cappuccio et al. 2020b; di Stefano et al. 2023). In addition, the high-accuracy accelerometer (HAA) will allow calibration of the main non-gravitational disturbances on radio tracking measurements, such as the ones due to propellant sloshing. The main scientific goal of the 3GM gravity experiment is the characterization of the interior structure of Ganymede and Callisto, with a focus on the properties of a possible subsurface liquid ocean. To accomplish this goal, the main physical quantities to be measured are the static gravity field of each moon, time-variable gravity, characterized by the tidal Love numbers, rotational parameters, and orbits. The flybys of Callisto, Europa, and Ganymede will also constrain the state vectors of the moons, which are crucial for the generation of precise ephemerides. A much more precise determination of the orbit of Ganymede in the Jovian system will be possible when JUICE

enters into a low-altitude orbit around the moon. The determination of the ephemerides of the Galilean moons will be supported by the PRIDE experiment, which will provide complementary VLBI data (Dirkx et al. 2017). Although lacking dedicated instrumentation, as in the case of JUICE/3GM, the Europa Clipper Gravity/Radio Science (G/RS) investigation will exploit the onboard radio subsystem to estimate the static and time-variable gravity field of Europa, its rotational state, and orbits in order to retrieve information about its interior structure and evolution (Mazarico et al. 2023).

The spacecraft can be tracked with three fanbeam (FB) antennas, two low-gain antennas (LGA), one MGA, and one HGA. All antennas are body-fixed and can only be oriented using the spacecraft itself. The radio subsystem supports both an X and Ka-band for downlink, coherent to an X-band uplink signal. Although the X/Ka link can provide both ranging and coherent Doppler, it is only available on the HGA. A Europa-nadir-pointed attitude will be adopted during each flyby, making it necessary to switch between the other available antennas during the 4-h gravity science window around the closest approach (C/A), in some cases more than once. However, the HGA will be available during navigation tracking passes, which will be placed approximately 12–28 h before and after the flyby.

During JUICE and Europa Clipper missions, range and Doppler tracking data will be used to perform an accurate orbit reconstruction of both spacecraft, allowing the retrieve the static gravity field and tidal parameters of the moons, together with their rotational states and orbits. As described in Sect. 1, the orbital evolution of the satellites will also provide crucial information about Jupiter's tidal parameters; in particular the dissipation at the frequency of the Galilean moons. A detailed characterization of the tidal interactions between Jupiter and the Galilean moons may provide crucial information about the origin, stability, and evolution of the Laplace resonance between the three innermost Galilean moons, with implications as to their habitability. In particular the Io–Jupiter interaction dominates the evolution of the Laplace resonance, as it is the body with the largest dissipation of the Galilean moons given its vicinity to Jupiter (Lainey et al. 2009; Lari et al. 2020), and evaluating the dynamics of Io is crucial in order to assess the direction of the evolution of the Laplace resonance.

The JUICE and Europa Clipper missions are each necessarily limited. JUICE will observe the orbit of Ganymede in exceptional detail thanks to its circular orbit phase (GCO), and will provide good information on Callisto's orbit thanks to 21 flybys of the moon, but little information about Europa. On the other hand, Europa Clipper will precisely constrain the orbit and gravity of Europa. Neither of the missions will make close encounters of Io.

Hence, a joint analysis of the data from the two missions can potentially improve the reconstruction of the gravity fields and ephemerides of all the Galilean moons, including Io, enhancing the scientific return of both missions

3. Dynamical model

Given the measurement accuracies expected from JUICE and Europa Clipper, a remarkably precise dynamical modelling of the accelerations acting on the spacecraft and on the moons is required to accurately reconstruct their orbits. The dynamical model for both the spacecrafts and the Galilean moons takes into account the gravitational interactions with the Sun, the planets, the Moon, Pluto, the asteroids, and the following moons of Jupiter: Io, Europa, Ganymede, Callisto, Metis, Thebe, Adrastea, and Amalthea. The planets, Pluto, the asteroids, and the satellites other than the Galilean moons are considered as point masses, taking into account the relativistic parameterized post-Newtonian first-order correction (Moyer 2005). The contribution of the nonspherical static gravity of Jupiter and the Galilean moons is expressed using a spherical harmonic expansion:

$$U(r,\phi,\lambda) = \frac{\mu}{r}\left(\sum_{l=2}^{\infty}\sum_{m=0}^{l}\overline{P}_{lm}(\sin(\phi))\left(\frac{R}{r}\right)^{l} \times\left(\overline{C}_{lm}\cos(m\lambda)+\overline{S}_{lm}\sin(m\lambda)\right)\right), \quad (9)$$

where μ is the gravitational parameter of the nonspherical body; R is the reference radius; r, ϕ, and λ are the radial distance, latitude, and longitude of the point where the potential is to be evaluated, respectively; $\overline{P}_{lm}$ is the fully normalized associated Legendre function of degree l and order m; and $\overline{C}_{lm}$ and $\overline{S}_{lm}$ are the fully normalized spherical harmonic coefficients.

Equation (9) takes into account only the static part of the potential. The tides exerted by an external body k produce time-varying corrections to the spherical harmonics coefficients, in particular for degree-2 (Petit & Luzum 2010):

$$\Delta\overline{C}_{2m} - i\Delta\overline{S}_{2m} = \frac{k_2}{5}\frac{\mu_k}{\mu}\left(\frac{a_e}{r_k}\right)^3\overline{P}_{2m}(\sin(\phi_k))\,e^{-im\lambda_k}, \quad (10)$$

where k_2 denotes the degree-2 Love number and it is implicitly assumed that k_2=k_{20}=k_{21}=k_{22}; μ_k denotes the gravitational parameter of the perturbing body; a_e denotes the mean equatorial radius of the tide body; and r_k, ϕ_k, and λ_k are the radial position, latitude, and longitude of the perturbing body seen by the body-fixed reference frame of the tide body, corrected for tidal bulge lag time Δt.

The total tide is raised by a set of perturbing bodies: in the case of Jupiter, these are the Galilean moons, while in the case of the moons, the perturbing body is Jupiter. In this analysis, the contribution by one moon to the tides raised on the other moons is neglected, as these are not relevant for the parameters studied in this work.

The potential in Eq. (9), with coefficient corrections from Eq. (10), represents the interaction between the figure of an extended body and a point mass: at any time, the gravitational acceleration of the body i – which is considered as a point mass – due to the extended body j is (Park et al. 2021):

$$\mathbf{a}_{\mathbf{i}(pm(i)-ext(j))} = \nabla\left(U_j(\mathbf{r_{ij}})\right), \quad (11)$$

where $\mathbf{r_{ij}}$ is the vector pointing from body j to body i. In addition, if i is also an extended body, the interaction between the nonspherical part of the body i and the body j considered as a point mass induces a gravitational acceleration on the body i itself – which we call self-oblateness – given by:

$$\mathbf{a}_{\mathbf{i}(ext(i)-pm(j))} = -\left(\frac{\mu_j}{\mu_i}\right)\nabla\left(U_i(\mathbf{r_{ji}})\right). \quad (12)$$

Instead, the figure-to-figure interaction can be considered negligible, even for the accuracy of the JUICE measurement (Dirkx et al. 2016). Therefore, the total gravitational acceleration acting on body i is:

$$\mathbf{a_{ij}} = \sum_{j\neq i}\mathbf{a}_{\mathbf{i}(pm(i)-ext(j))} + \mathbf{a}_{\mathbf{i}(ext(j)-pm(i))}. \quad (13)$$

The integration is typically evaluated in an inertial frame, and thus the gravitational acceleration computed in the body-fixed frame must be rotated into the inertial frame (e.g., EME2000).

The force received by a body i from the tides it raises on an extended body j can be written as (Mignard 1980):

$$\mathbf{F}_{ij} = -\frac{3G(k_2)_j M_i^2 R_j^5}{r_{ij}^8}\left(\mathbf{r}_{ij} + (\Delta t)_j\left[\frac{2\mathbf{r}_{ij}\left(\mathbf{r}_{ij}\mathbf{v}_{ij}\right)}{r_{ij}^2}\right]\right), \tag{14}$$

where $\mathbf{\Omega}$, is the spin velocity vector, R the radius, and Δt the tidal bulge lag time.

The time lag Δt is defined by:

$$\Delta t = T \arctan(1/Q)/2\pi, \tag{15}$$

where T is the period of the main tidal excitation. For the tides raised by the central body on a satellite, T is equal to $2\pi/n$, where n is the mean motion of the satellite. For the tides raised on the central body by a satellite, T is equal to $2\pi/2(\Omega - n)$, where Ω is the spin frequency of the central body. And the force received by the extended body i induced by its own tides raised by j can be written as:

$$\mathbf{F}_{ij} = \frac{3\,(k_2)_i\, G(M_j^2)\,(R_i)^5}{r_{ji}^8} \times\left(\mathbf{r}_{ji} + (\Delta t)_i\left[\frac{2\mathbf{r}_{ji}\left(\mathbf{r}_{ji}\mathbf{v}_{ji}\right)}{r_{ji}^2} + \left(\mathbf{r}_{ji}\times\mathbf{\Omega_i} + \mathbf{v}_{ji}\right)\right]\right). \tag{16}$$

We note that Eqs. (14) and (15) apply in principle also to satellite-to-satellite tides, which will be measured by 3GM in the Ganymede phase (De Marchi et al. 2022). In Eq. (16), it can be seen that the dissipative part of the tidal force depends on the rotation of the tide body and therefore also on its self-oblateness acceleration due to static gravity field. Hence, particular care must be taken in the modeling of the rotational state of the moons.

The Galilean moons, as in most of the natural satellites of the Solar System, are assumed to be in synchronous rotation, meaning that the orbital and rotational periods are the same and the spin axis is perpendicular to the orbital plane (the so-called spin–orbit resonance; see e.g. Murray & Dermott 1999). In this state, the permanent bulge would ideally always point to the empty focus of the orbit. In reality, because of internal dissipations in the body's interior, the triaxiality of the body, and third-body perturbations, the long axis of the body librates (to first order in eccentricity) around the empty focus of the nearly Keplerian orbit (physical libration; Van Hoolst et al. 2020). This forced libration is expected to be the combination of multiple oscillations at different frequencies (Rambaux et al. 2011). Moreover, the spin axis of the body could be tilted with respect to the orbital plane by an angle called obliquity. However, the obliquity of the Galilean moons is believed to be very small, albeit not yet observed (Baland et al. 2012). We modeled the orientation of the satellites as Lainey et al. (2019): the spin axis $\hat{z}$ is oriented as the instantaneous angular momentum vector, i.e. $\hat{z} = \frac{r\times v}{|r\times v|}$. Then, the prime meridian X is computed from the direction of the central planet through a rotation around Z by the angle:

$$\gamma = -2e\sin M + A\sin M, \tag{17}$$

where e and M are the instantaneous eccentricity and mean anomaly, respectively, and A is the amplitude of the physical libration, which is assumed to be zero a priori but is estimated as part of the radio science experiment.

However, in an N-body problem with strongly coupled dynamics, as in the Galilean moons, the spin axis and, more importantly, the prime meridian would undergo periodic oscillations due to the perturbations of the instantaneous orbital plane and empty focus, potentially affecting the orbital evolution. As modeling the rotational dynamics of the satellites is particularly complex – as it depends on the rheology, composition, and structure of the body, and as the rotational model of Io cannot be retrieved directly by JUICE or Europa Clipper –, we decided to remove the effects of the rotation in the tidal modeling and implemented the simplified model adopted by Lari (2018):

$$\mathbf{F}_{ij} = \frac{3\,(k_2)_i\, G(M_j^2)\,(R_i)^5}{r_{ji}^8}\left(\mathbf{r}_{ji} + (\Delta t)_i\left[7\frac{\mathbf{r}_{ji}\left(\mathbf{r}_{ji}\mathbf{v}_{ji}\right)}{r_{ji}^2}\right]\right). \tag{18}$$

In short, we substitute the librational tides, which are dependent on the body's rotation, with four-thirds of the radial tide in order to keep the total tidal energy dissipation constant (Murray & Dermott 1999). However, in addition to the effects on the orbits of the moons, their rotational states directly affect the motion of the spacecraft through the orientation of their gravity fields. Hence, to take into account the uncertainties in the rotational state in the estimation of the gravity fields of the moon, we estimated an offset in the pole orientation – parameterized by right ascension and declination angles – in addition to the physical libration amplitude. For this reason, the forces acting on the spacecraft due to the tides on the moons are computed from Eq. (10).

In summary, the tides influence the trajectory of the spacecraft – and therefore also the radiometric data – in two ways: directly, through the effect of a time-variable gravity on the spacecraft, computed using Eq. (10); and indirectly, through the effect on the orbital motion of the moons, computed using Eqs. (18) and (10). In the estimation process, we constrain the tidal bulge lag time Δt of the two models to be the same.

For a covariance analysis, this approach can be considered sufficient; however, future work is needed to develop and test a coherent tidal model for the spacecraft and the moons, possibly taking into account the coupling between rotational and orbital dynamics for Europa, Ganymede, and Callisto, given the quantity and quality of data from JUICE and Clipper.

In our simulation, we also integrated the orbit of the Jupiter barycenter around the Sun to take into account the uncertainty of the position of Jupiter and therefore the possible systematic errors on range measurements. In this case, we only considered the gravitational forces of the bodies external to the Jupiter system. In the dynamical model, we also considered the solar radiation pressure (SRP), the largest of the nongravitational accelerations acting on the spacecraft, considering its exact shape.

4. Numerical simulations

In this work, we performed numerical simulations of JUICE and Europa Clipper orbit determination using MONTE (Mission-analysis, Operations, and Navigation Tool-kit Environment; (Evans et al. 2018), an orbit determination software toolkit developed by JPL that has been used for nearly two decades for data analysis of navigation and radio science experiments of deep space missions (Park et al. 2016, 2020; Durante et al. 2019, 2022; Iess

et al. 2018). Our goal is to perform a covariance analysis to retrieve the expected accuracies for the estimation of the main gravitational parameters governing the dynamics of the Jovian system.

As described in Dirkx et al. (2017), uncertainties estimated with a covariance analysis can be optimistic with respect to real errors, because of possible dynamical mismodeling and unmodeled biases and correlations in the measurements. This issue can be mitigated by considering conservative assumptions on the noise of the data and increasing the number of parameters in the estimation. Hence, it must be stressed that the real uncertainties obtained with the real data analysis will probably be different from those provided in this paper, especially because of the complexity of the dynamical modeling of the system.

In the following subsections, we provide a brief overview of the orbit determination method used for this investigation, the details of the observable used, including the assumptions on the expected noises, and finally the parameters that our estimation filter solves.

4.1. Methods

The process of orbit determination aims at reconstructing the past evolution of the spacecraft trajectory. To this aim, it is necessary to estimate dynamical parameters that influence the spacecraft trajectory, including the gravity fields and the orbits of the celestial bodies. The most common approach adopts a batch weighted square-root information filter (Bierman 2006) that minimizes the weighted difference between the real measurements (the so-called "observed observables") and the synthetic measurements computed by means of a dynamical and an observation model (the so-called "computed observables") (Moyer 2005).

For a nonlinear system, the solution is iterative, and the differential correction at k-th step is:

$$\hat{\mathbf{x}}_{\mathbf{k+1}}=\hat{\mathbf{x}}_{\mathbf{k}}-\left(A_k^T W A_k+P_0^{-1}\right)^{-1}\left(A_k^T W\left(\mathbf{z}-\hat{\mathbf{z}}\left(\hat{\mathbf{x}}_{\mathbf{k}}\right)\right)+P_0^{-1}\left(\mathbf{x_0}-\hat{\mathbf{x}}_{\mathbf{k}}\right)\right), \tag{19}$$

where $\hat{\mathbf{x}}_{\mathbf{k+1}}$ is the estimated state vector at the end of the kth iteration, A_k is the partial derivative computed with respect to the estimated parameters at the kth iteration, z is the vector of the observed observables, $\hat{\mathbf{z}}\left(\hat{\mathbf{x}}_{\mathbf{k}}\right)$ is the vector of the computed observables at the kth iteration, W is the measurement-weighting matrix (i.e., assumed to be the inverse of the covariance matrix of the measurements noise), $\mathbf{x_0}$ is the a priori knowledge of the state vector, and P_0 is the a priori covariance matrix.

In addition, the covariance matrix of the estimated parameters is:

$$P_k=\left(A_k^T W A_k+P_0^{-1}\right)^{-1}. \tag{20}$$

In a simulation environment, the observed observables are also synthetic, and are usually generated using the same models of the computed observables with the addition of a realistic noise based on the current best prediction of the noise we expect to encounter during the missions. Therefore, the estimated and the a priori state vectors coincide, and the only meaningful output is the covariance matrix of the estimation. This process is called covariance analysis.

The dynamical model of the spacecraft is not completely deterministic, which is due to the fact that our probe is significantly affected by complex nongravitational accelerations (Milani & Gronchi 2010). Given that gravity radio science investigations usually use data from different flybys separated in time by weeks or months, we use a multi-arc approach (Tortora et al. 2016; Zannoni et al. 2020; Durante et al. 2020; Iess et al. 2019) to overcome the nondeterministic nature of the orbit determination problem (Serra et al. 2018). In this approach, the entire time span of the observations is decomposed into short nonoverlapping and noncontiguous intervals usually centered at the C/A of the flybys. In the case of the circular orbit phase around Ganymede, we simply divide it into many adjacent intervals (Cappuccio et al. 2020a). Each arc will have its own set of observables and its initial conditions, and therefore we estimate a set of local parameters independently for each arc. In addition, the global parameters, such as the gravity parameters (see Sect. 4.3), are common to all arcs.

4.2. Observables

For our analysis, we assumed the JUICE reference trajectory – labeled 150la according to the nomenclature used by the project – described in CReMa 5.0 (ESA SPICE Service 2018). Regarding the Jupiter tour, we took into account 2 flybys of Europa, 4 flybys of Ganymede, and 21 flybys of Callisto, considering arcs of 48 h centered on the C/A. For the Ganymede eccentric orbital phase, we considered only 3 arcs of 24 h centered around the pericenters below 1000 km in altitude. Finally, we considered 135 consecutive arcs of 24 h to cover the five-month circular orbital phase at 500 km altitude (GCO500). During this phase, JUICE will be in a quasi-polar orbit, with a mean inclination of 97 degrees. In this study, we did not consider the final circular orbital phase at 200 km altitude (GCO200), which is currently envisioned for the later part of the mission. This will provide global coverage of Ganymede's gravity field at higher resolution, becoming by far the most detailed and accurate among the Galilean moons (Cappuccio et al. 2020a). From Fig. 1, it can be seen that the flybys provide a good coverage of Callisto, both in longitude and latitude, which is useful to better sample both zonal and sectorial gravity harmonics.

JUICE is endowed with a triple radio link configuration at two frequency bands (X/X, X/Ka, and Ka/Ka), which will allow for a full calibration of dispersive noise sources (Bertotti et al. 2003; Mariotti & Tortora 2013). Regarding the ground antennas, we considered the ESTRACK Deep Space Network, assuming that, when the Jupiter tour starts, all stations will support the Ka-band both for uplink and downlink.

Currently, only the Malargue station has this capability. Moreover, we assume that the path delay induced by Earth's troposphere can be calibrated using the water vapor radiometers at the ESTRACK stations currently under development (Lasagni Manghi et al. 2021, 2023). In this tracking configuration, the end-to-end Doppler accuracy is expected to be, in terms of Allan deviation, $\sim 1 \times 10^{-14}$ at 1000 s integration time. During the GCO phase, we consider approximately 7 h of tracking a day, considering the Malargue station only. Regarding JUICE's noise assumptions, we followed the experiment requirements and the BepiColombo performance (Lasagni Manghi et al. 2023; Cappuccio et al. 2020a), as the latter carries the same transponder as JUICE. We simulated only two-way Doppler and range data, considering an Allan deviation (ADEV) of 1×10^{-14} at 1000 s integration time, corresponding to Doppler measurements with an accuracy of 12 $\mu m\,s^{-1}$ at 60 s integration time. The count time of Doppler data was chosen as 60 s as a trade-off between the sensitivity to gravity spherical harmonics and numerical error considerations (Zannoni & Tortora 2013).

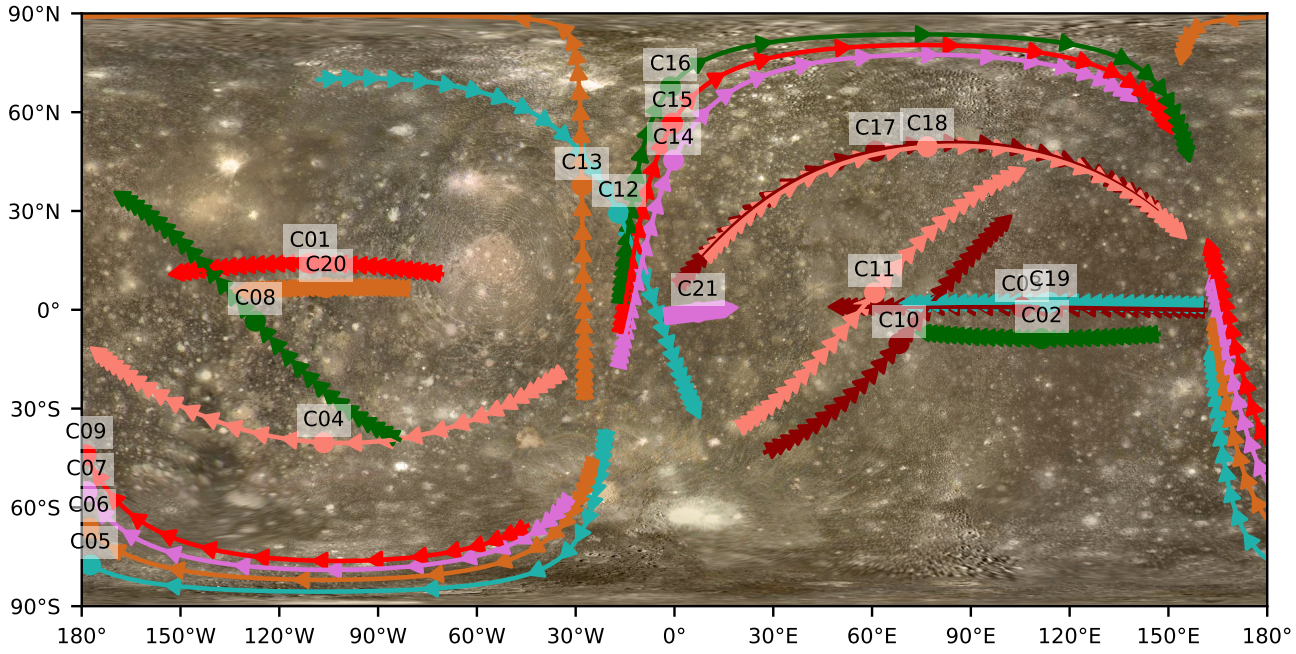

Fig. 1. Ground tracks of the flybys planned by JUICE over Callisto. The ground tracks are represented over a map of Callisto produced using Galileo and Voyager images produced by Björn Jónsson.

Regarding Europa Clipper, we considered the 21F31 v4 as the reference trajectory (see Campagnola et al. (2019) for a general description of the tour design). The baseline mission comprises 53 flybys of Europa, providing a good coverage both in longitude and latitude (Fig. 2). There will also be 8 flybys of Ganymede and 9 of Callisto, but they are not part of the baseline mission for science investigations.

As mentioned in Sect. 2, we consider 4 h of tracking around the closest approach of the flybys exploiting the antenna, among the LGAs and FBs, which provides the highest signal-to-noise ratio (SNR). Only two-way X/X Doppler observations with SNR above 4 dB-Hz are considered, as in Mazarico et al. (2023). Because of the absence of a multifrequency link during the C/A passes, dispersive noise, such as solar plasma, cannot be calibrated. In addition, during some passes, the Io plasma torus is expected to produce a nondynamical Doppler shift that may produce a bias in the estimation if not properly calibrated (Moirano et al. 2021). Calibrations may be generated using models (Phipps et al. 2018; Moirano et al. 2021). In this work, we assume a complete calibration of the Io plasma torus. However, removing or de-weighting the data that may be affected by the IPT affects mainly the estimation of the Europa gravity field, while the expected uncertainty in the dissipation parameters increases negligibly. In addition to the data during the C/A, we will also exploit the standard navigation tracking passes, which are scheduled to be approximately 12–28 h before and after the closest approaches. During these tracking windows, two-way Doppler and range will be generated using the HGA. Range data will be acquired in X/X only, while X/X and X/Ka tracking links may be possible for Doppler data. The Doppler noise level adopted in the simulations was computed using empirical models of the main noise sources (Iess et al. 2014; Mazarico et al. 2023) and is represented in Fig. 3. In general, this noise level mainly depends on spacecraft electronics, ground station instrumentation, Earth's atmosphere delay, and the Sun–Earth–Probe (SEP) angle during flybys. The noise increases considerably during solar conjunctions, when the SEP angle decreases below 10 degrees. In this condition, the solar plasma becomes the dominant source of noise. The average noise during the C/A is expected to be around 100 $\mu m\,s^{-1}$ at 60 s integration time, which is almost eight times the noise expected for the JUICE mission, while it is expected to improve by a factor of about 2, that is, to 50 $\mu m\,s^{-1}$ at 60 s, when using the HGA. For the two-way range data, a 1 m noise jitter and a systematic error of 2 m were considered. For both JUICE and Europa Clipper, in the simulation of the observables, we adopt a minimum spacecraft elevation angle of 15 degrees from the station to account for errors that might affect low-elevation calibration data for Earth's troposphere. In addition, we consider the occultation of the spacecraft by Jupiter and the Galilean moons.

4.3. Filter setup

Our simulation aims at determining the uncertainty achievable for the ephemerides of the Galilean moons during the time span of Juice and Europa Clipper and for the main dissipative parameters of the moons and Jupiter, which are parameterized by the imaginary part of the Love number k_2. To do so, we performed a global estimation of the main parameters of the moons and Jupiter, including the most important parameters influencing the orbit determination of the spacecraft. Table 1 summarizes the parameters estimated in our setup.

We estimated the antenna offset during the flybys of JUICE and Europa Clipper because the motion of the antenna phase center with respect to the center of mass of the spacecraft induces a Doppler shift in the signal; this effect can be relevant during tracking with LGA/FBA, but is usually negligible with the HGA.

The estimated range biases take into account residual systematic errors, which are considered constant for each tracking pass. To take into account possible mismodelings in the dynamical model, we also solved for empirical piecewise-constant accelerations uncorrelated in time and estimated in batches of 8 h. We assumed the value of $\mathrm{Im}(k_2)$ of the moons and $\mathrm{Im}(k_2)$ of Jupiter to be zero, as their nominal values do not influence the

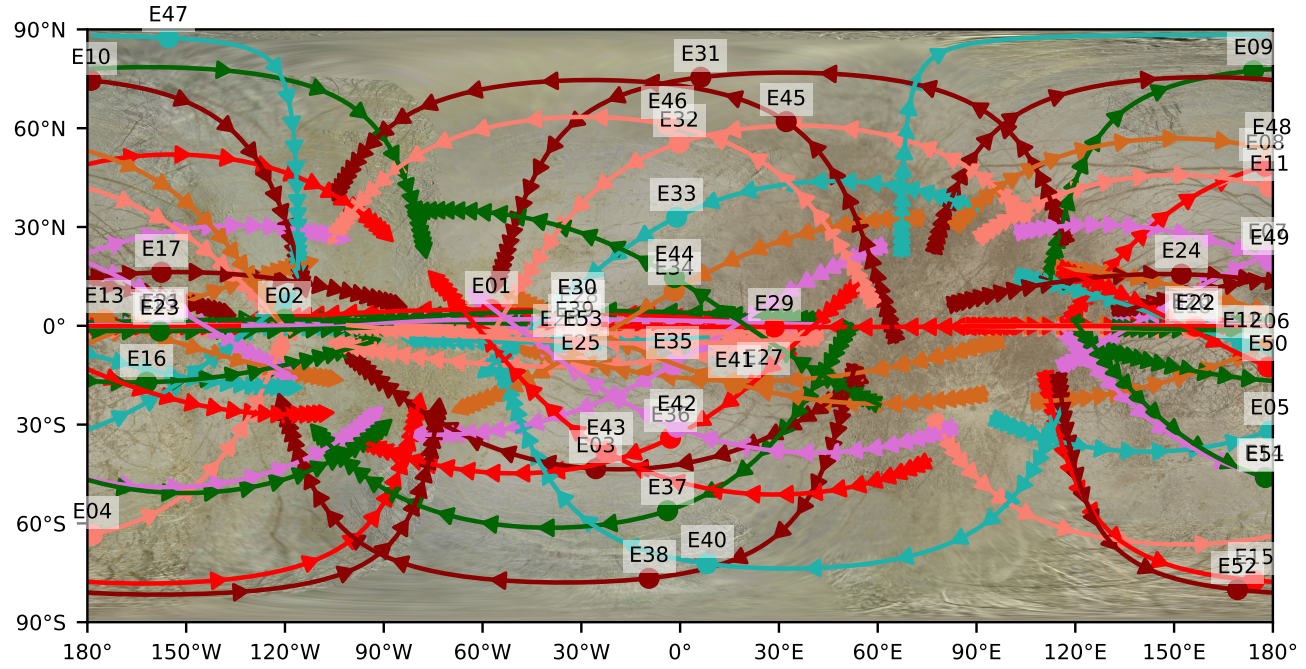

Fig. 2. Ground tracks of the flybys planned by Europa Clipper over Europa. The ground tracks are represented over a map of Europa produced using Galileo and Voyager images produced by Björn Jónsson.

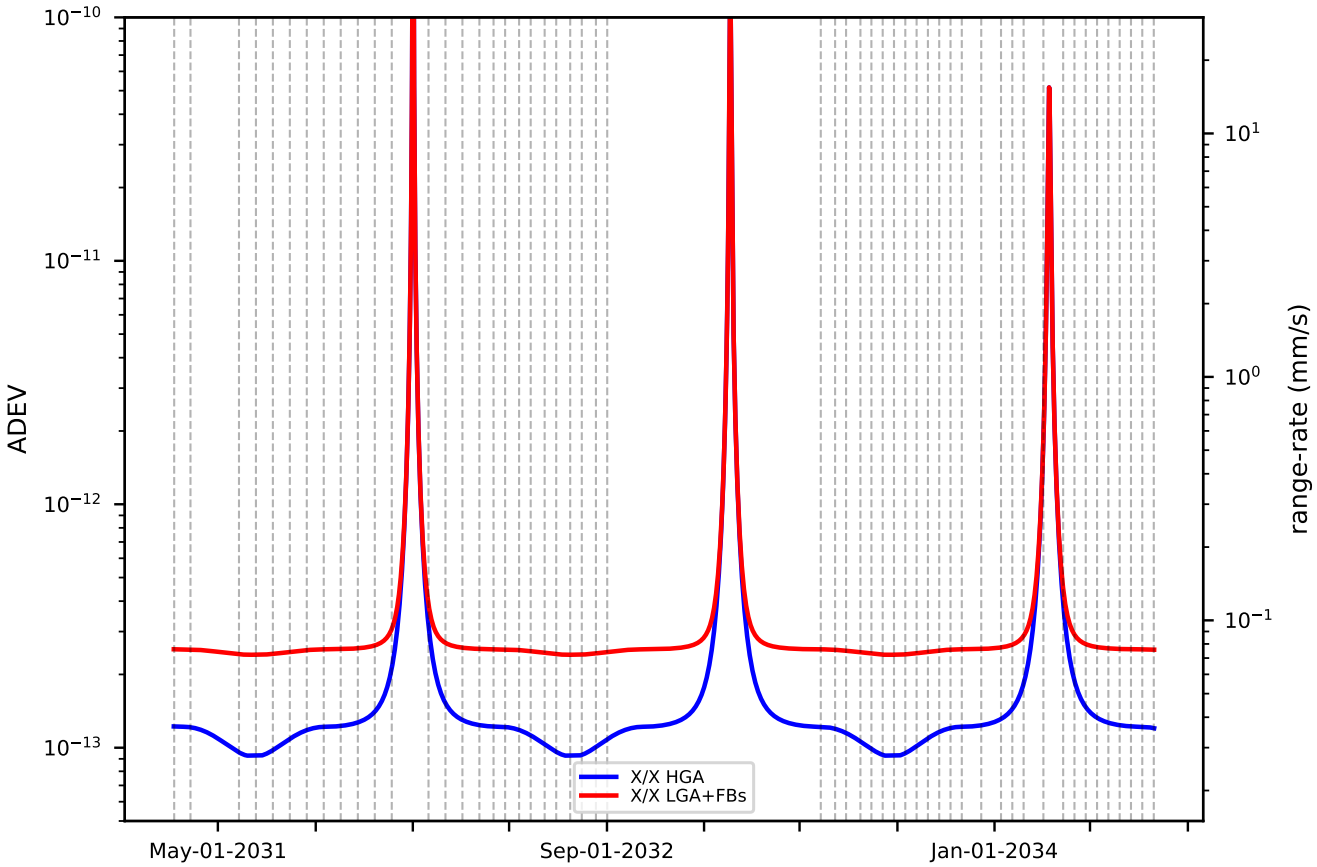

Fig. 3. Expected Doppler noise during the Europa Clipper mission – at an integration time of 60 s – in terms of Allan standard deviation (left) and two-way range rate (right). The expected noise during the FBs and LGA tracking is shown in red, and the noise using the HGA is shown in blue. The vertical dashed lines represent the Europa Clipper flybys of Europa.

Table 1. Simulation setup of the joint analysis JUICE and Europa Clipper.

Spacecraft (local parameters)		
Parameter	Nominal values and specifications	A priori uncertainty
State	Initial states from CReMA 5.0 (JUICE) and 21F31 v4 (Europa Clipper)	Unconstrained
Antenna phase offsets	Nominal value: 0 m.	1 m for X, Y, Z directions
SRP scale factor	Solar radiation pressure scaling factor set to 1.0	0.5
Range bias	Nominal value: 0 m.	JUICE: 1 m Europa Clipper: 2 m
Empirical accelerations	Nominal value: 0 km/s^2.	1.5×10^{-12} km/s^2
Galilean moons (global parameters)		
Parameter	Nominal values and specifications	A priori uncertainty
Satellites state	Epoch at 01-JAN-2033, initial state from jup380	Unconstrained
GMs	GMs of the Galilean moons and innermost moons of Jupiter from JPL's jup380 (ftp://ssd.jpl.nasa.gov/pub/eph/satellites/bsp/jup380s.bsp)	Unconstrained
Europa's gravity harmonics coefficients	Quadrupole coefficients from Gomez Casajus et al. (2021), higher terms simulated from Kaula's rule, $K = 2.0 \times 10^{-5}$. Estimated up to order and degree 15.	Degree-2 unconstrained, higher terms Kaula's rule with $K = 10 \times 10^{-5}$
Ganymede's gravity harmonics coefficients	Quadrupole coefficients from Gomez Casajus et al. (2022), higher terms simulated from Kaula's rule, $K = 0.9 \times 10^{-5}$. Estimated up to order and degree 50.	Degree-2 unconstrained, higher terms Kaula's rule with $K = 4.5 \times 10^{-5}$
Callisto's gravity harmonics coefficients	Quadrupole coefficients from Anderson et al. (2001), higher terms simulated from Kaula's rule, $K = 1.125 \times 10^{-5}$. Estimated up to order and degree 9.	Degree-2 unconstrained, higher terms Kaula's rule with $K = 5.625 \times 10^{-5}$
Tidal parameters	Estimated Re(k_2) and Im(k_2) for all the Galilean moons. Re(k_2) from Lainey et al. (2009), Mazarico et al. (2023), Cappuccio et al. (2022).. Im(k_2) nominal value: 0.	Unconstrained
Rotational state	Estimated libration amplitudes at orbital period and pole obliquity as right ascension and declination of the rotational axis of Europa, Ganymede and Callisto.	Libration amplitudes unconstrained, Right ascension and Declination = 0.5 deg
Jupiter (global parameters)		
Parameter	Nominal values and specifications	A priori uncertainty
State	With respect to the Sun. Epoch at 01-JAN-2033, initial state from DE440.	Unconstrained
GM and gravity harmonics coefficients	From Durante et al. (2020). Estimated zonal harmonics coefficients up degree 6.	Juno results ×100 (Durante et al. 2020)
Tidal parameters	Re(k_2) from Durante et al. (2020).. Im(k_2) nominal value: 0.	Unconstrained
Rotational state	From Archinal et al. (2018). Assuming linear model for pole's right ascension, declination and prime meridian.	Unconstrained

resulting uncertainties. Jupiter's Re(k_2) is assumed equal at all frequencies, as they are expected to be very close in value (Wahl et al. 2020) and because we do not expect to be sensitive to the different values from JUICE and Europa Clipper data.

In order to estimate Jupiter's Im(k_2) we followed two approaches: (1) assuming a different Jupiter's Im(k_2) for each Galilean moon (frequency-dependent approach), which is considered the most realistic model as shown by Fuller et al. (2016), Lainey et al. (2017, 2020); (2) assuming a constant Jupiter's Q (and so Im) for all the Galilean moons, as assumed in Lainey et al. (2009), in order to perform a direct comparison with their results.

Regarding the gravity coefficients of the moons which are greater than degree-2, in accordance with Cappuccio et al. (2022) and Mazarico et al. (2023), we built a synthetic field using Kaula's rule (Kaula 1966). The Kaula factor of each satellite K (Bills et al. 2014) was derived from Titan's value, retrieved by Durante et al. (2019), according to the formula:

$$K \cong K_t \left(\frac{GM_t}{GM}\right)^{\frac{2}{3}}, \tag{21}$$

where K_t is the Kaula's factor of Titan, M_t is the mass of Titan, M is the target body's mass, and G is the gravitational constant.

5. Results

5.1. Gravity and tidal parameters of the moons

The focus of this work is on the ephemerides of the Galilean moons and the tidal dissipation in the Jupiter system. In this section, we therefore only briefly address the gravity analysis of the

Table 2. Io's and Europa's degree-2 tidal parameter uncertainties achievable by JUICE, Clipper, and the joint analysis (1σ).

Europa	A priori sigma	Mazarico et al. (2023)	JUICE	Clipper	JUICE+Clipper	$\sigma_{J+EC}/\sigma_{EC}$
Re(k_2)	Unconstr.	0.0047 – 0.009	2.03	0.0052	0.0045	0.86
Im(k_2)	Unconstr.		0.07	0.0051	0.0042	0.83
Io		Lainey et al. (2009)				
Im(k_2)	Unconstr.	3.0×10^{-3}	4.5×10^{-2}	2.9×10^{-2}	$(0.13 – 1.6) \times 10^{-2}$	0.04

Notes. The adopted a priori uncertainties are shown in the second column. For comparison, the third column reports the expected uncertainties for Europa Clipper from Mazarico et al. (2023) for Europa, while Lainey et al. (2009) for Io. The range reported for Mazarico et al. (2023) do not take into account the corrective coefficient considered in Table 5 of Mazarico et al. (2023). The column "$\sigma_{J+EC}/\sigma_{EC}$" represents the ratio between the uncertainty of JUICE+Clipper and that of Europa Clipper-only.

Galilean moons, with a focus on a comparison to previous analyses and the improvements allowed by the combination of JUICE and Europa Clipper data.

Our current knowledge of the gravity field of the Galilean moons comes from the analysis of Galileo and Juno radio tracking data and optical images. Galileo radio tracking data were acquired at S-band only due to a failure in the deployment of the HGA, while the Juno spacecraft acquired both X- and Ka-band data. Galileo performed 7 flybys of Io, 11 of Europa, and 8 of Ganymede and Callisto, although not every flyby was considered in the published gravity analysis due to problems with the tracking link. Juno has so far performed 1 flyby of Ganymede and 1 of Europa. The limited number of flybys of Juno and the tracking limitations of Galileo allowed to estimate only the quadrupole of the static gravity field of the Galilean moons could be estimated (Anderson et al. 2001; Gomez Casajus et al. 2022, 2021; Schubert et al. 2004). No tidal parameter results have yet been published from the analysis of these data.

Cappuccio et al. (2020a, 2022) showed that the analysis of JUICE tracking data is expected to vastly improve the current knowledge of Ganymede's and Callisto's gravity fields thanks to the large number of flybys, the orbital phase, and the state-of-the-art tracking system. In particular, the quadrupole uncertainty of Ganymede could be improved by about two orders of magnitude, and the gravity field could be measured up to degree and order 35–45. In addition, the quadrupole of Callisto could be improved by about one order of magnitude, with an estimation up to degree and order 7. The tidal parameters of Ganymede, both the real and imaginary parts, will be estimated with exquisite precision thanks to the GCO phase, while for Callisto, the uncertainty retrieved for the Re(k_2) could allow an unambiguous detection of an ocean, but no strong constraint will be obtained on the imaginary part. Our JUICE-only results are fully compatible with these published results, considering the same assumptions.

Thanks to the excellent coverage and precision of JUICE data, we find that the addition of Europa Clipper data does not improve the gravity recovery for Ganymede and Callisto. A marginal improvement is possible by adding the Doppler data acquired during the navigation flybys of Ganymede and Callisto, as discussed in more detail in Sect. 5.5. The nominal results shown in Table 2 and the following section regarding Jupiter's tidal parameters take into account only the baseline Europa Clipper mission scenario, that is, only the 53 flybys of Europa are considered.

Regarding Europa, Mazarico et al. (2023) showed the results achievable by Europa Clipper using only 4 h of Doppler data acquired with LGA/FBA around the closest approach. These authors estimated Europa's static gravity field up to degree and order 20 and the Re(k_2), showing that a global field could be measured up to degree 8–10 (depending on the assumption about the gravity field strength) and that the current knowledge about Europa's quadrupole is expected to improve by approximately an order of magnitude. Considering the same tracking assumptions, our results are fully compatible. The inclusion of JUICE data allowed an additional improvement of about 30% for J_2 and 25% for C_{22} thanks to the superior tracking performance of JUICE and the relatively low flyby altitude (400 km).

Table 2 shows the results of JUICE, Europa Clipper, and the joint analysis, that is the attainable accuracies in the degree-2 tidal parameters of Io and Europa. For comparison purposes, the single-mission solutions consider the same estimation setup as the joint analysis, assuming a constant Jupiter Im(k_2) for all the moons. However, the joint analysis results for Europa's tidal parameters are not significantly affected by the estimation assumption about Jupiter's Im(k_2). As can be seen in Table 2, the improvement by adding JUICE data to Clipper is ~15% for Europa's degree-2 tidal parameters.

In case of an ocean beneath Europa's ice shell, current theoretical models predict a Re(k_2) of about 0.23 (Mazarico et al. 2023) and a phase lag of up to 1° (Moore & Schubert 2000), which corresponds to an Im(k_2) of ~0.004. However, in extreme cases, with partial melt in Europa's silicate mantle similar to Io's state, the phase lag can reach values of up to ~25° (Hussmann et al. 2016), which corresponds to an Im(k_2) of 0.09. Without a global subsurface ocean, Re(k_2) would be reduced to <40.015 and the Im(k_2) would stay close to the lower limit shown above (Moore & Schubert 2000).

Therefore, the accuracy achievable on both Re(k_2) and Im(k_2) by JUICE and Europa Clipper may be sufficient to confirm the presence of a liquid ocean. However, a detailed characterization of the internal structure of Europa, including ocean density and ice shell thickness and rigidity, would require a global inversion of all available measurements, including tidal Love numbers k_2 and h_2, static gravity field, topography, and magnetic induction (Wahr et al. 2006; Durante et al. 2019; Petricca et al. 2023).

Regarding Io, Lainey et al. (2009) provided the only published direct estimation of a tidal parameter of a Galilean moon. Io's k_2/Q was determined to be 0.015 ± 0.003 using an extensive set of astrometric ground observations between 1891 and 2007, and including observations of the mutual events from 1973 to 2003.

The effect of Im(k_2) on the dynamics accumulates over time linearly in the radial direction and quadratically in the tangential direction, and so the longer the time span of observations, the better it can be estimated. Despite the fact that JUICE and Europa Clipper will not fly by Io, its tidal parameter Im(k_2) can be estimated from the evolution of the orbital motion of the other moons, especially Europa, thanks to the Laplace resonance. As mentioned in Sect. 1, having a good estimation of this parameter is crucial in order to understand the stability and evolution of the

Table 3. Jupiter's GM, degree-2 gravity, and tidal parameter uncertainties achievable by JUICE, Clipper, and the joint analysis (1σ).

Jupiter	A priori sigma	Durante et al. (2020)	Lainey et al. (2009)	JUICE (Q constant)	Europa Clipper (Q constant)	JUICE+Clipper (Q constant)	JUICE+Clipper (freq. dep.)	Units
GM	2.8			0.303	0.327	0.175	0.186	km^3/s^2
J_2	56	0.56		17.93	24.44	4.93	5.11	$\times10^{-9}$
Re(k_2)	50	0.6		2.15	18.15	1.25	1.26	$\times10^{-2}$
Im(k_2)	Unconstr.		0.020	0.20	0.12	**0.011**		$\times10^{-4}$
Im(k_2) (Io)	Unconstr.						0.210	$\times10^{-4}$
Im(k_2) (Eur)	Unconstr.						13.02	$\times10^{-4}$
Im(k_2) (Gan)	Unconstr.						1.57	$\times10^{-4}$
Im(k_2) (Cal)	Unconstr.						**40.10**	$\times10^{-4}$

Notes. The adopted a priori uncertainties are shown in the second column. For comparison, the third and fourth columns report the uncertainties from Durante et al. (2020) and Lainey et al. (2009).

Laplace resonance, as among the Galilean moons, Io is the body with the largest dissipation due to its proximity to Jupiter.

In order to make a direct comparison with Lainey et al. (2009), in Table 2, for the result of Io's Im(k_2), we show the expected uncertainty of the joint analysis obtained considering a constant Im(k_2) for all the moons equal to that of Jupiter (result on the left), as well as considering a frequency-dependent estimation (result on the right).

We expect an improvement by a factor of about 3 with respect to Lainey et al. (2009) for Im(k_2). This is mainly due to the higher accuracy of radio science data with respect to astrometric data, which allows a better sensitivity to the dynamical effects of Im(k_2) in a much shorter interval of time. As can be seen in Table 2, most of the information comes from Europa Clipper data, as Europa is much more influenced by Io's orbit. Instead, considering a frequency-dependent Im(k_2) of Jupiter, the uncertainty in the Im(k_2) of Io increases by an order of magnitude (the reason for this is explained in Sect. 5.3).

5.2. Gravity and tidal parameters of Jupiter

The formal uncertainties (1σ) on the estimated parameters for Jupiter retrieved from our analyses can be found in Table 3, together with some relevant current knowledge. Durante et al. (2020) estimated the gravity field of Jupiter from the radiometric data of 17 perijove passes of the Juno mission, both static (up to degree 30) and dynamic up to degree and order 4, real part only). As expected, the joint analysis of JUICE and Europa Clipper will not be able to improve the uncertainties of the J_2 and Re(k_2) for Jupiter, because Juno is directly sampling the gravity of the planet from a privileged orbit during its low altitude pericenter passes (about 4000 km above the cloud top), while JUICE and Europa Clipper can only retrieve Jupiter gravity indirectly from the orbits of the moons.

As mentioned in Sect. 1, the imaginary part of the Jovian Love number Im(k_2) is a key parameter for evaluating the orbital evolution of the Galilean moons and the Laplace resonance stability. In particular, assuming a constant Q at the frequencies of all the moons, as in Lainey et al. (2009), the Im(k_2) can be retrieved with an expected accuracy of 1.1×10^{-6}, which is a factor of about 2 better than what has been published so far.

When comparing the results of the single mission estimations, even if the radiometric data accuracy is lower, we see that Europa Clipper provides a stronger information content on Jupiter's Im(k_2) with respect to JUICE, because the orbital motion of Europa is more sensitive to the orbit of Io.

However, the most realistic approach may be to consider a frequency-dependent estimation, because the tidal dissipation within a planet can strongly depend on the satellite that raises the tides (Fuller et al. 2016; Lainey et al. 2017, 2020). As expected, the best accuracy can be achieved on Jupiter's Im(k_2) at Io's frequency, because it dominates the dissipation and the orbital evolution of all the satellites locked in the Laplace resonance. A frequency-dependent estimation increases the uncertainly on Jupiter's Im(k_2) at the frequency of Io by more than one order of magnitude with respect to a single-frequency estimation. This is mainly due to the correlation between the Im(k_2) at the frequencies of Io and Europa, as discussed in Sect. 5.3.

Finally, assessing the dissipation at Callisto's frequency can be crucial for reconstructing the past and future of the Laplace resonance, and in particular the duration of its existence, with consequences for the potential habitability of the Galilean moons. Lari et al. (2023) found that, assuming the dissipation in Jupiter at the frequency of Callisto to be negligible, as expected from classical tidal theory, Ganymede will reach a 2:1 resonance with Callisto about 1.5 billions of years from now. The resonance locking theory presented by Fuller et al. (2016) proposes instead that the dissipation of Jupiter at the frequency of Callisto could be very high ($Q \sim 1$); if it were, Callisto would indeed be the satellite with the highest migration rate of the system. In this case, Lari et al. (2023) demonstrated that, in the majority of their simulations, the occurrence of the 2:1 mean motion resonance between Ganymede and Callisto could plausibly have taken place in the past. This resonance would emerges as a driver of the evolution of the Laplace resonance, due to the redistribution of Callisto's angular momentum among the moons in resonance. While this resonance ultimately disintegrated, different configurations of the Galilean moons during that era could result in distinct durations and evolutions of this complex four-body resonance.

Our simulation results on Jupiter's Im(k_2) at the frequency of Callisto correspond to a Q uncertainty of ~0.02, assuming $Q = 1$. Considering higher values that still fall outside the range predicted by classical theory, $Q = 10$ and $Q = 100$, we obtain uncertainties of 0.7 and 68, respectively. Therefore, the joint JUICE and Europa Clipper analysis may detect the presence of the resonance locking mechanism between Jupiter and Callisto.

Jupiter's Im(k_2) at the frequency of the three innermost Galilean moons are expected to be close in magnitude, in absence of resonance in Jupiter's interior (Lari et al. 2020; Fuller et al. 2016). Constraining them to be the same, the estimation of Jupiter's Im(k_2) at the frequency of Callisto (Im(k_2)(Callisto))

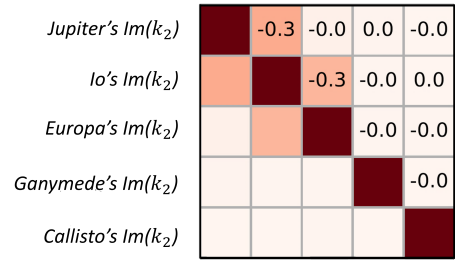

Fig. 4. Correlation matrix of the dissipative parameters of Jupiter (constant Q) and those of the moons.

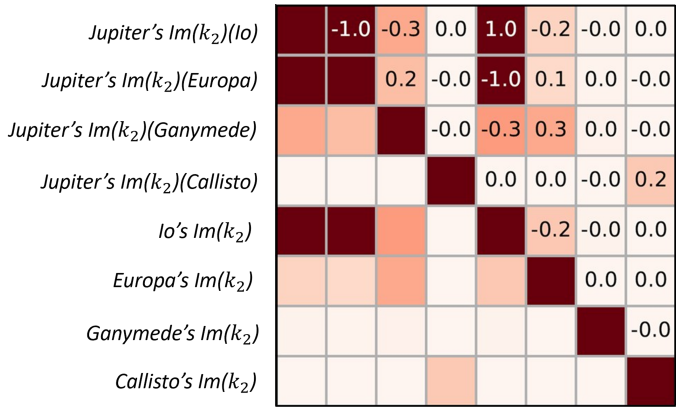

Fig. 5. Correlation matrix of the dissipative parameters of Jupiter at the frequencies of the Galilean moons and those of the moons.

improves negligibly with respect to the unconstrained result shown in Table 3.

5.3. Correlations between Love numbers

As explained in Sect. 1, the secular effect of the tidal dissipation within a moon on its orbit is very similar to the effect of the dissipation inside Jupiter at the frequency of that moon (Malhotra 1991; Lainey et al. 2009). Hence, we expect a high correlation between the estimates of tidal dissipation parameters derived from the orbital motion. This could make the independent estimation of the two parameters solely from the effects on the orbital evolution quite difficult (Lainey et al. 2009). However, when multiple moons are present, the tidal bulge raised by a moon on the central planet causes small long-period effects on the orbits of the other moons. These "cross-direct" effects are much smaller than the direct ones, but their different behavior can help to decorrelate the tidal dissipation within the planet and the satellite, provided sufficient accuracy to detect them.

Figure 4 reports the expected correlations between the Im(k_2) of Jupiter and its satellites in the constant Q scenario. As can be seen, the correlation between the Im(k_2) of Jupiter and Io is relatively low (–0.3). Indeed, the improved accuracies provided by the JUICE and Europa Clipper joint analysis enable the detection of the cross-direct effects of the tidal bulge raised by Io on the orbits of Europa or Ganymede. Indeed, in a simulation where the cross-direct effects are removed, the correlation becomes close to 1. Furthermore, the decorrelation does not come from the constant Q constraint, as the same decorrelation is observed if only Jupiter's Im(k_2) at the frequency of Io is estimated. As expected, the Im(k_2) of Jupiter is not correlated with those of Europa, Ganymede, and Callisto, as the tides of Jupiter are dominated by Io. A relatively small correlation (0.3) can be observed between the Im(k_2) of Io and Europa. This is caused by the fact that the tidal dissipation within Io is estimated indirectly, mainly through the effects that the dynamics of Io has on the orbital motion of Europa. Figure 5 shows the expected correlations between the tidal dissipation parameters of Jupiter and its moons, as obtained by our joint analysis with a frequency-dependent approach.

In this case, we find a strong correlation (–1.0) between Jupiter's Im(k_2) at the frequency of Io and Io's Im(k_2). In fact, using a frequency-dependent approach, a strong correlation emerges between the Im(k_2) of Jupiter at the frequencies of Io and Europa, again due to the indirect observation of Io's state from Europa's orbit, together with the strong coupling from the Laplace resonance. This prevents the detection of the cross-direct tidal effects. This high correlation is also the reason why the Io Im(k_2)–Jupiter Im(k_2)(Io) and Io Im(k_2)–Jupiter Im(k_2)(Europa) correlations are almost equal (close to 1). Moreover, it is the cause of the large increase in the uncertainties of Io's Im(k_2) and Jupiter's Im(k_2)(Io) between a frequency-dependent and a constant Q estimation, which increase by factors of approximately 10 and 20, respectively, as shown in Tables 2 and 3. Despite the frequency-dependent approach, we do not observe any significant correlation between the Im(k_2) of the other moons and that of Jupiter at the corresponding frequency. We find that this decorrelation comes from the sampling of the gravity of the moons during the flybys of JUICE and Europa Clipper, which, thanks to the precision of the radio signals, are sensitive to the tides of the moons, including the Im(k_2), from the direct influence they have on the spacecraft trajectory. This enables an independent estimation of Jupiter's Im(k_2) at the respective frequency, estimated solely from the orbital effect on the moon. Indeed, removing the influence of the tides on the spacecraft and keeping only the effects on the moons' orbits, the correlation between the Im(k_2) of each moon and that of Jupiter at the respective frequency would reach values close to 1. For these reasons, a mission focused on Io (Keane et al. 2021) and the joint analysis with missions like Juno and Galileo could be crucial for the estimation of the dissipation in the Jupiter system.

5.4. Satellite ephemerides

In this section, we present the expected formal uncertainties on the orbits of the Galilean moons achievable with this joint analysis. In addition, we provide a comparison with the results obtainable by the single missions in order to evaluate the contribution of a joint analysis to the estimation, considering a single Im(k_2) for Jupiter. Figures 6 and 7 show the attainable accuracies for the ephemerides of the Galilean moons, comparing the best results coming from the single missions (left) and the joint analysis result (right) in order to highlight the synergies between the two missions (in Appendix A, the full covariance matrices are also shown). Table 4 summarizes the results.

As expected, we obtain the best accuracy in the radial direction, which is bounded by a stable value, while we are less sensitive in the normal direction. The transverse direction is coupled to the radial direction, and in general it degrades when no observations are available. The accuracy in the normal direction may be improved by adding VLBI observables, although their contribution in the radial and transverse directions is expected to be negligible (Dirkx et al. 2017).

Thanks to the Laplace resonance, knowledge of the orbit of just one of the three innermost Galilean moons provides information on the other two moons. A prime example is Io, for which we

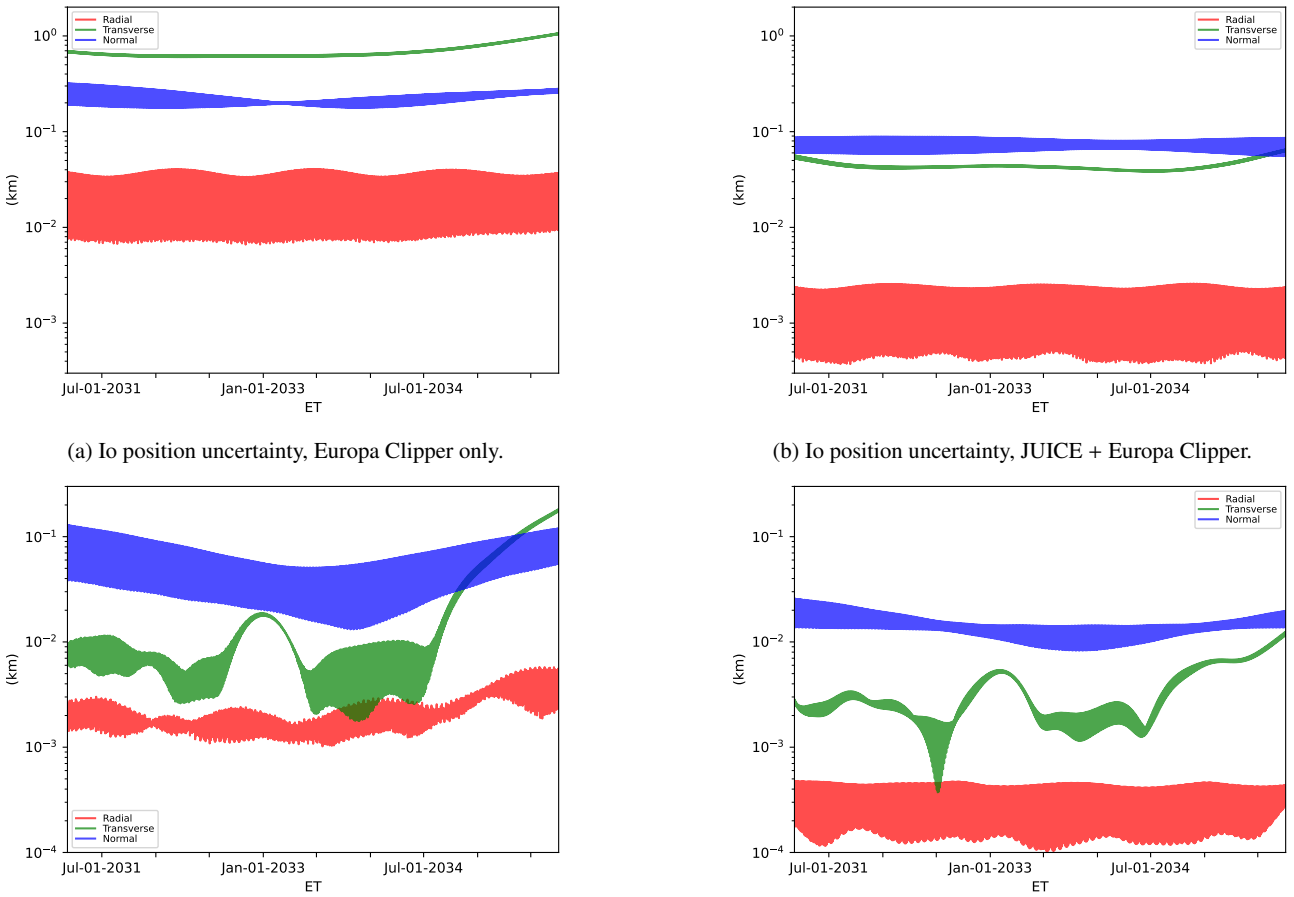

(a) Io position uncertainty, Europa Clipper only.

(b) Io position uncertainty, JUICE + Europa Clipper.

(c) Europa position uncertainty, Europa Clipper only.

(d) Europa position uncertainty, JUICE + Europa Clipper.

Fig. 6. Expected Io and Europa position uncertainties (1σ) in the radial, tangential, and normal to the orbital plane directions during the combined time spans of the JUICE and Europa Clipper missions with respect to the Jupiter Barycenter. The Europa Clipper-only solution is displayed on the left, with JUICE+Clipper on the right.

are able to retrieve good accuracy (see Table 4), even in the total absence of flybys, mainly from data provided by Europa Clipper, as explained in Sect. 5.1.

One of the most interesting synergies between the two missions concerns the ephemerides of Europa. Although JUICE will perform only two flybys, thanks to the Laplace resonance, it is able to provide a substantial improvement to the uncertainties in the joint analysis. Moreover, we note that the transverse direction uncertainty reaches its minimum at the time of the two JUICE flybys (2 and 16 July 2032).

As expected, the position uncertainties for Ganymede are the smallest, which is thanks to the JUICE GCO phase. The uncertainties are higher in the first part of the time span, because the GCO lasts from May 2035 to the end of the JUICE mission in October 2035.

Thanks to the precise orbit determination of Europa allowed by Europa Clipper, and the strong coupling between Europa and Ganymede, Europa Clipper improves the JUICE-only uncertainties by a factor of about two in the three directions. Finally, Callisto shows the best accuracy in the middle of the observation time span, when the majority of JUICE flybys occur. We note that the improvement of the joint analysis is limited with respect to the other moons, which is due to the fact that Callisto is not in resonance and therefore does not similarly benefit from the better knowledge of Europa and Ganymede.

5.5. Europa Clipper's Callisto flybys

As mentioned in Sect. 4.2, Europa Clipper will perform several flybys of Ganymede and Callisto as well. In particular, the trajectory considered in this work comprises of eight flybys of Ganymede and nine of Callisto.

The baseline concept of operations does not consider these flybys for the gravity investigation. However, radiometric data will likely be collected during the flybys for navigation purposes, and so it is interesting to evaluate how these data may contribute to the global solution. Hence, starting from the baseline joint analysis described in the previous sections, we added the Europa Clipper radiometric data during the Ganymede and Callisto flybys. We assumed that only Doppler data will be obtained with low-gain and fan-beam antennas at the closest approach, while Doppler and range during the flyby wings exploiting the HGA, similarly to what will be done during the Europa flybys.

As a first result, we find that the contribution to Ganymede static gravity, tides, and orbit is negligible because of the strong constraints already provided by JUICE GCO phase. Regarding Callisto, we obtain an improvement of ∼9% on J_2 and C_{22}, and ∼11% on Re(k_2) and Im(k_2).

Assuming that both Doppler and ranging data will be obtained with the HGA also at the closest approach, the

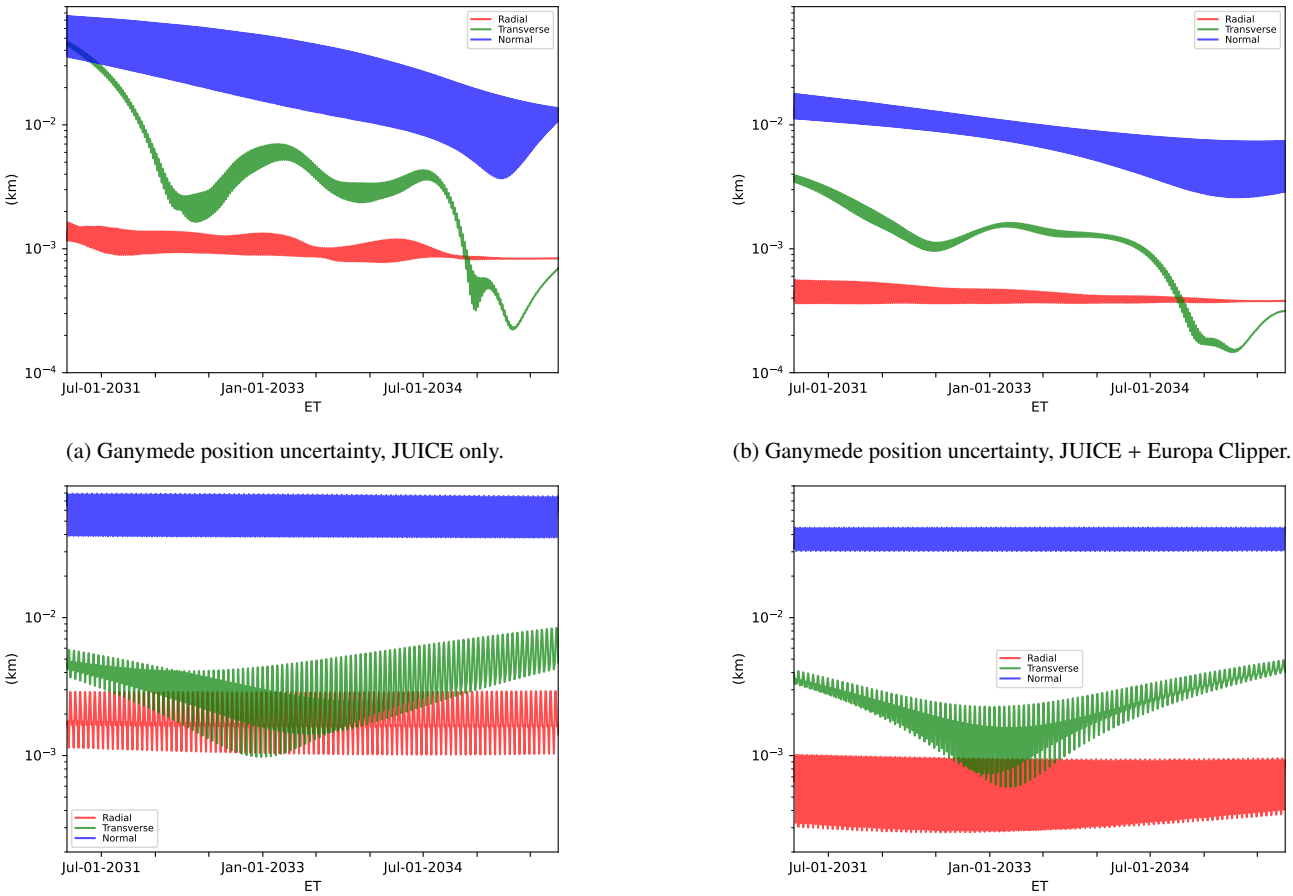

(a) Ganymede position uncertainty, JUICE only.

(b) Ganymede position uncertainty, JUICE + Europa Clipper.

(c) Callisto position uncertainty, JUICE only.

(d) Callisto position uncertainty, JUICE + Europa Clipper.

Fig. 7. Expected Ganymede and Callisto position uncertainties (1σ) in the radial, tangential, and normal to the orbital plane directions during the combined time spans of the JUICE and Europa Clipper missions with respect to the Jupiter Barycenter. The Europa Clipper-only solution is displayed on the left, with JUICE+Clipper on the right.

Table 4. Formal position uncertainties (1-σ) of the Galilean moons from the joint analysis JUICE + Europa Clipper in the radial, tangential, and normal to the orbital plane directions.

Formal position uncertainties (m)	Radial	Tangential	Normal
Io	0.6–2	70	80
Europa	0.1–0.5	0.5–10	15
Ganymede	0.4	0.2–4	4–15
Callisto	0.4–1	1–10	40

Notes. Approximate average values during the combined time spans of the missions are provided.

improvement with respect to the baseline will be ∼15% for J_2 and C_{22}, and ∼25% for Re(k_2) and Im(k_2).

The improvement is limited because of the higher Doppler noise level for Europa Clipper compared to JUICE, as explained in Sect. 4.2. Moreover, considering the current nominal trajectories, Europa Clipper will not improve the true anomaly distribution available from the JUICE tour, which is crucial for estimating Re(k_2), as shown in Fig. 8. Nevertheless, the pericenter and apocenter of Callisto's orbit around Jupiter are only covered by one JUICE flyby, and so the additional Europa Clipper data will improve the robustness and stability of the estimation.

Finally, we obtain only a ∼10% improvement for the Jupiter's Im(k_2), even at Callisto's frequency. This is mainly because the Europa Clipper Callisto flybys occur during the nominal time span of the JUICE mission, and therefore the overall estimation time span is not increased with respect to the baseline.

We note that both the JUICE and Europa Clipper tours are still undergoing optimization. It is likely that the output of this process will further improve the results of the gravity science and celestial mechanics investigations.

6. Conclusions

The main focus of this work is to study how the joint analysis of two-way range and Doppler data from the upcoming JUICE and Europa Clipper missions can improve our knowledge of the ephemerides of the Galilean moons, and of the tidal dissipation

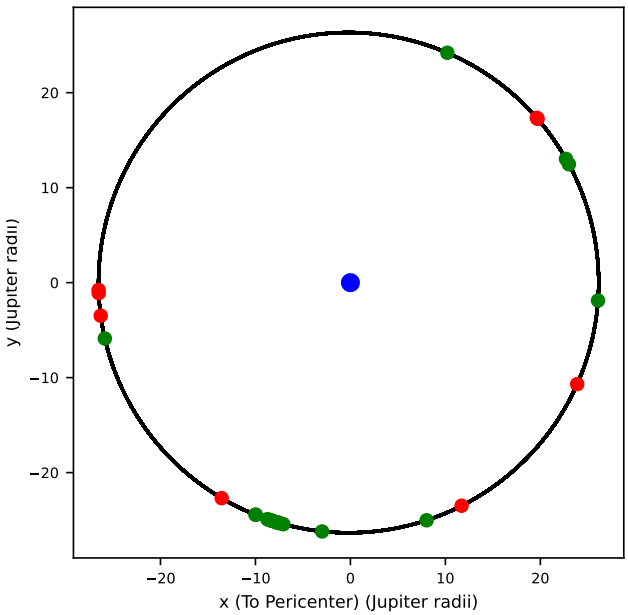

Fig. 8. Position of Callisto with respect to Jupiter during JUICE (green) and Europa Clipper (red) flybys shown in the orbital plane, where the X axis points to the pericenter of the orbit.

within the Jupiter system. Indeed, the dissipative phenomena, in particular between Jupiter and Io, are the root cause of the formation and evolution of the Laplace resonance involving the three innermost Galilean moons, with consequences on their habitability.

We evaluated the expected formal uncertainties of the main parameters influencing the orbit determination of the spacecraft and the estimation of the dissipative parameters of Jupiter's system through detailed numerical simulations of the orbit determination of the two spacecraft, taking into account the currently envisioned mission operations with realistic performance of the space and ground segments. First of all, we examined the gravity fields of the moons. Regarding Ganymede and Callisto, the addition of Europa Clipper radiometric data is not expected to improve the results of JUICE (Cappuccio et al. 2020a, 2022), because the current baseline concept of operations for Europa Clipper gravity investigation is to acquire tracking data only during the flybys of Europa. Adding the tracking data during Europa Clipper's flybys of Callisto is expected to bring an improvement of about 25% in the Re(k_2) and Im(k_2), and ∼10% in the Jupiter Im(k_2)(Callisto) in the best scenario. Even though the expected improvement is limited, Europa Clipper's flybys would increase the robustness and the reliability of the estimation of Callisto's gravity, especially in case of problems during the JUICE flybys around Callisto's pericenter and apocenter.

For Europa, we found that the addition of the two JUICE flybys allows improvement of the degree-2 tidal parameters by ∼15% with respect to an analysis with Europa Clipper only. Regarding Io, ase no direct flyby of the moon will be performed by JUICE or Europa Clipper, we estimated only its degree-2 tides, from the dynamical influence of its orbital evolution on Europa and Ganymede. The uncertainty in the Im(k_2) of Io is expected to be 1.3×10^{-3}, almost a factor 3 smaller than that achieved so far (Lainey et al. 2009), considering the same assumption of a constant Q in Jupiter for all the Galilean moons. In a frequency-dependent estimation of Jupiter's Love numbers, the uncertainty in the Im(k_2) of Io increases by an order of magnitude, to 1.6×10^{-2}.

We then focused on the estimation of the dissipative parameters of Jupiter at the frequencies of the Galilean moons. We find that the joint analysis is expected to improve our knowledge of the Jupiter–Io tidal dissipation. In particular, the accuracy in the Im(k_2) of Jupiter could be 1.1×10^{-6}, a factor of about 2 better than that achieved previously Lainey et al. (2009), again with the assumption of a constant Q in Jupiter for all the Galilean moons. This interesting result can be obtained even though the total time span covered by the JUICE and Europa Clipper missions is less than 5 yr, which is much shorter than the ∼120 yr analyzed by Lainey et al. (2009), because of the high accuracy of the radiometric measurements. When considering a more realistic frequency-dependent tidal dissipation within Jupiter, the expected uncertainty in Jupiter's Im(k_2)(Io) increases by a factor about 20 with respect to the constant Q estimation, mainly due to the correlation between the different frequencies of Jupiter's Love numbers.

Regarding Jupiter's Im(k_2)(Callisto), we obtain an uncertainty of 4.0×10^{-3}, corresponding to an uncertainty on Q of ∼ 0.02, 0.7, or 68 assuming $Q = 1$, 10, or 100, respectively, which would allow the detection of a resonance locking mechanism between Callisto and Jupiter, as theorized by Fuller et al. (2016).

As expected we see a strong correlation (close to 1) between Jupiter's Im(k_2)(Io) and Io's Im(k_2), and also between Jupiter's Im(k_2)(Io) and Im(k_2)(Europa), because the majority of the information we have about Io's dynamics comes from its effect on Europa, which is precisely determined by Europa Clipper radio tracking data.

We do not see any significant correlation between the Love numbers of Europa, Ganymede, and Callisto and that of Jupiter at the corresponding frequency. This de-correlation comes from the direct sampling of the gravity of the moons by JUICE and Clipper. For this reason, a mission dedicated to the study of Io could be crucial for the estimation of the dissipation in the system.

Moreover, we presented the uncertainties on the recovery of the Io, Europa, Ganymede, and Callisto positions in the radial, transverse and normal directions, considering a single Im(k_2) for Jupiter. As expected, the Ganymede ephemerides are the most accurate, given the JUICE GCO phase. In general, the ephemerides of the Galilean moons can be potentially recovered with an accuracy of less than 1 m in the radial direction, a few meters in the transverse – except for Io for which the accuracy is ∼70 m –, and tens of meters in the normal direction. Interestingly, this level of accuracy for Io can be reached even without any flyby of the moon, thanks to its strong coupling with Europa and Ganymede through the Laplace resonance. In general, the joint JUICE and Europa Clipper analysis allows to greatly improve the reconstruction of the ephemerides with respect to the single missions. Probably the most interesting synergy is the contribution of JUICE to the orbit of Europa. Even though JUICE will perform only two flybys of this moon, we expect an improvement of a factor 2–5 in the three directions, thanks also to the very precise knowledge of Ganymede's orbit during the GCO phase and the Laplace resonance.

In summary, the joint analysis of the radio tracking data of the future missions JUICE and Europa Clipper has the potential to greatly contribute to the estimation of the Jovian system ephemerides and tidal dissipation, highlighting a strong synergy between the two missions.

Acknowledgements. A.M., M.Z., L.G.C., P.T. and L.I. acknowledge financial support from the Italian Space Agency through the Agreements 2023-6-HH.0 (JUICE), 2022-16-HH.0 (BepiColombo annd Juno) and 2021-13-HH.0 (Europa Clipper). A part of this work was performed at the Jet Propulsion Laboratory, California Institute of Technology, under a contract with the National Aeronautics and Space Administration.

References

Anderson, J., Jacobson, R., McElrath, T., et al. 2001, Icarus, 153, 157
Archinal, B., Acton, C., A'hearn, M., et al. 2018, Celest. Mech. Dyn. Astron., 130, 1
Baland, R. M., Yseboodt, M., & Van Hoolst, T. 2012, Icarus, 220, 435
Bertotti, B., Iess, L., & Tortora, P. 2003, Nature, 425, 374
Bierman, G. J. 2006, Space Sci. Rev., 213, 5
Bills, B. G., Asmar, S. W., Konopliv, A. S., Park, R. S., & Raymond, C. A. 2014, Icarus, 240, 161
Bolton, S. J., Lunine, J., Stevenson, D., et al. 2017, Space Sci. Rev., 213, 5
Campagnola, S., Buffington, B. B., Lam, T., Petropoulos, A. E., & Pellegrini, E. 2019, J. Guidance Control Dyn., 42, 2615
Cappuccio, P., Hickey, A., Durante, D., et al. 2020a, Planet. Space Sci., 187, 104902
Cappuccio, P., Notaro, V., di Ruscio, A., et al. 2020b, IEEE Trans. Aerospace Electron. Syst., 56, 4984
Cappuccio, P., Di Benedetto, M., Durante, D., & Iess, L. 2022, Planet. Sci. J., 3, 199
Cassen, P., Reynolds, R. T., & Peale, S. J. 1979, Geophys. Res. Lett., 6, 731
De Marchi, F., Cappuccio, P., Mitri, G., & Iess, L. 2022, Icarus, 386, 115150
Dirkx, D., Lainey, V., Gurvits, L., & Visser, P. 2016 Planet. Space Sci., 134, 82
Dirkx, D., Gurvits, L. I., Lainey, V., et al. 2017, Planet. Space Sci., 147, 14
di Stefano, I., Cappuccio, P., & Iess, L. 2023, J. Spacecraft Rockets, 60, 5
Durante, D., Hemingway, D., Racioppa, P., Iess, L., & Stevenson, D. 2019, Icarus, 326, 123
Durante, D., Parisi, M., Serra, D., et al. 2020, Geophys. Res. Lett., 47, e2019GL086572
Durante, D., Guillot, T., Iess, L., et al. 2022, Nat. Commun., 13, 4632
Efroimsky, M., & Lainey, V. 2007, J. Geophys. Res.: Planets, 112, E12003
Efroimsky, M., & Makarov, V. V. 2013, ApJ, 764, 26
Evans, S., Taber, W., Drain, T., et al. 2018, CEAS Space J., 10, 79
Fayolle, M., Magnanini, A., Lainey, V., et al. 2023, A&A, 677, A42
Fuller, J., Luan, J., & Quataert, E. 2016, MNRAS, 458, 3867
Goldreich, P., & Sciama, D. 1965, MNRAS, 130, 159
Gomez Casajus, L. G., Zannoni, M., Modenini, D., et al. 2021, Icarus, 358, 114187
Gomez Casajus, L., Ermakov, A. I., Zannoni, M., et al. 2022, Geophys. Res. Lett., 49, e2022GL099475
Grasset, O., Dougherty, M. K., Coustenis, A., et al. 2023, Planet. Space Sci., 78, 1
Howell, S. M., & Pappalardo, R. T. 2020, Nat. Commun., 11, 1311
Hussmann, H., Shoji, D., Steinbrügge, G., Stark, A., & Sohl, F. 2016, Celest. Mech. Dyn. Astron., 126, 131
Iess, L., & Boscagli, G. 2001, Planet. Space Sci., 49, 1597
Iess, L., Jacobson, R. A., Ducci, M., et al. 2012, Science, 337, 457
Iess, L., Di Benedetto, M., James, N., et al. 2014, Acta Astron., 94, 699
Iess, L., Folkner, W. M., Durante, D., et al. 2018, Nature, 555, 220
Iess, L., Militzer, B., Kaspi, Y., et al. 2019, Science, 364, eaat2965
ESA SPICE Service 2018, JUICE Operational SPICE Kernel Dataset, https://doi.org/10.5270/esa-ybmj68p
Kaula, W. M. 1964, Rev. Geophys., 2, 661
Kaula, W. M. 1966, Theory of Satellite Geodesy. Applications of Satellites to Geodesy (Waltham, Mass.: Blaisdell)
Keane, J., Ahern, A. A., Bagenal, F., et al. 2021, Bull. AAS, 53, 179
Lainey, V., Arlot, J.-E., Karatekin, Ö., & Van Hoolst, T. 2009, Nature, 459, 957
Lainey, V., Jacobson, R. A., Tajeddine, R., et al. 2017, Icarus, 281, 286
Lainey, V., Noyelles, B., Cooper, N., et al. 2019, Icarus, 326, 48
Lainey, V., Casajus, L. G., Fuller, J., et al. 2020, Nat. Astron., 4, 1053
Lari, G. 2018, Celest. Mech. Dyn. Astron., 130, 50
Lari, G., & Milani, A. 2019, Planet. Space Sci., 176, 104679
Lari, G., Saillenfest, M., & Fenucci, M. 2020, A&A 639, A40
Lari, G., Saillenfest, M., & Grassi, C. 2023, MNRAS, 518, 3023
Lasagni Manghi, R., Zannoni, M., Tortora, P., et al. 2021, Radio Sci., 56, e2021RS007330
Lasagni Manghi R., Bernacchia, D., Gomez Casajus, L., et al. 2023, Radio Sci., 58, e2022RS007614
Lee, M. H., & Peale, S. J. 2002, ApJ, 567, 596
Lieske, J. 1998, A&ASS, 129, 205
Malhotra, R. 1991, Icarus, 94, 399
Mariotti, G., & Tortora, P. 2013, Radio Sci., 48, 111
Mazarico, E., Buccino, D., Castillo-Rogez, J., et al. 2023, Space Sci. Rev., 219, 30
Mignard, F. 1980, Moon Planets, 23, 185
Milani, A., & Gronchi, G. 2010, Theory of Orbit Determination (Cambridge University Press)
Mitri, G., Meriggiola, R., Hayes, A., et al. 2014, Icarus, 236, 169
Moirano, A., Gomez Casajus, L., Zannoni, M., Durante, D., & Tortora, P. 2021, J. Geophys. Res.: Space Phys., 126, e2021JA029190
Moore, W. B., & Schubert, G. 2000, Icarus, 147, 317
Moyer, T. D. 2005, Formulation for Observed and Computed Values of Deep Space Network Data Types for Navigation (John Wiley and Sons Ltd.)
Murray, C. D., & Dermott, S. F. 1999, Solar System Dynamics (Cambridge University Press)
Musotto, S., Varadi, F., Moore, W., & Schubert, G. 2002, Icarus, 159, 500
Palumbo, P., Jaumann, R., Cremonese, G., et al. 2014, EGU General Assembly 2014, held 27 April - 2 May, 2014 in Vienna, Austria, 10227
Park, R. S., Asmar, S. W., Buffington, B. B., et al. 2011, Geophys. Res. Lett., 38, L24202
Park, R. S., Bills, B., Buffington, B. B., et al. 2015, Planet. Space Sci., 112, 10
Park, R. S., Konopliv, A. S., Bills, B. G., et al. 2016, Nature, 537, 515
Park, R. S., Konopliv, A. S., Ermakov, A. I., et al. 2020, Nat. Astron., 4, 748
Park, R. S., Folkner, W. M., Williams, J. G., & Boggs, D. H. 2021, AJ, 161, 105
Peale, S. J., & Cassen, P. 1978, Icarus, 36, 245
Petit, G., & Luzum, B. 2010, IERS Conventions, IERS Tech. Note, 36
Petricca, F., Genova, A., Castillo-Rogez, J. C., et al. 2023, Geophys. Res. Lett., 50, e2023GL104016
Phipps, P. H., Withers, P., Buccino, D. R., & Yang, Y. M. 2018, J. Geophys. Res.: Space Phys., 123, 6207
Rambaux, N., Van Hoolst, T., & Karatekin, Ö. 2011, A&A, 527, A118
Serra, D., Spoto, F., & Milani, A. 2018, Celest. Mech. Dyn. Astron., 130, 1
Schubert, G., Anderson, J. D., Spohn, T., & McKinnon, W. B. 2004, Jupiter: Planet Satellites Magnetosphere, 1, 281
Tortora, P., Zannoni, M., Hemingway, D., et al. 2016, Icarus, 264, 264
Tobie, G., Mocquet, A., & Sotin, C. 2005, Icarus, 177, 534
Van Hoolst, T., Baland, R.-M., Trinh, A., Yseboodt, M., & Nimmo, F. 2020, J. Geophys. Res.: Planets, 125, e2020JE006473
Wahl, S. M., Parisi, M., Folkner, W. M., Hubbard, W. B., & Militzer, B. 2020, ApJ, 891, 42
Wahr, J. M., Zuber, M. T., Smith, D. E., & Lunine, J. I. 2006, J. Geophys. Res.: Planets, 111
Witte, M., & Savonije, G. 1999, A&A, 350, 129
Yoder, C. F., & Peale, S. J. 1981, The tides of Io, Icarus, 47, 1
Zannoni, M., & Tortora, P. 2013, J. Guidance Control Dyn., 36, 1008
Zannoni, M., Hemingway, D., Casajus, L. G., & Tor- tora, P. 2020, Icarus, 345, 113713

Appendix A: Covariance matrices of moon states

In this Appendix, we show the full correlation matrices for single missions and a joint analysis of the states of the moons, whose uncertainties are shown in Section 5.4, together with the dissipative parameters, considering a constant Q estimation for Jupiter's tides.

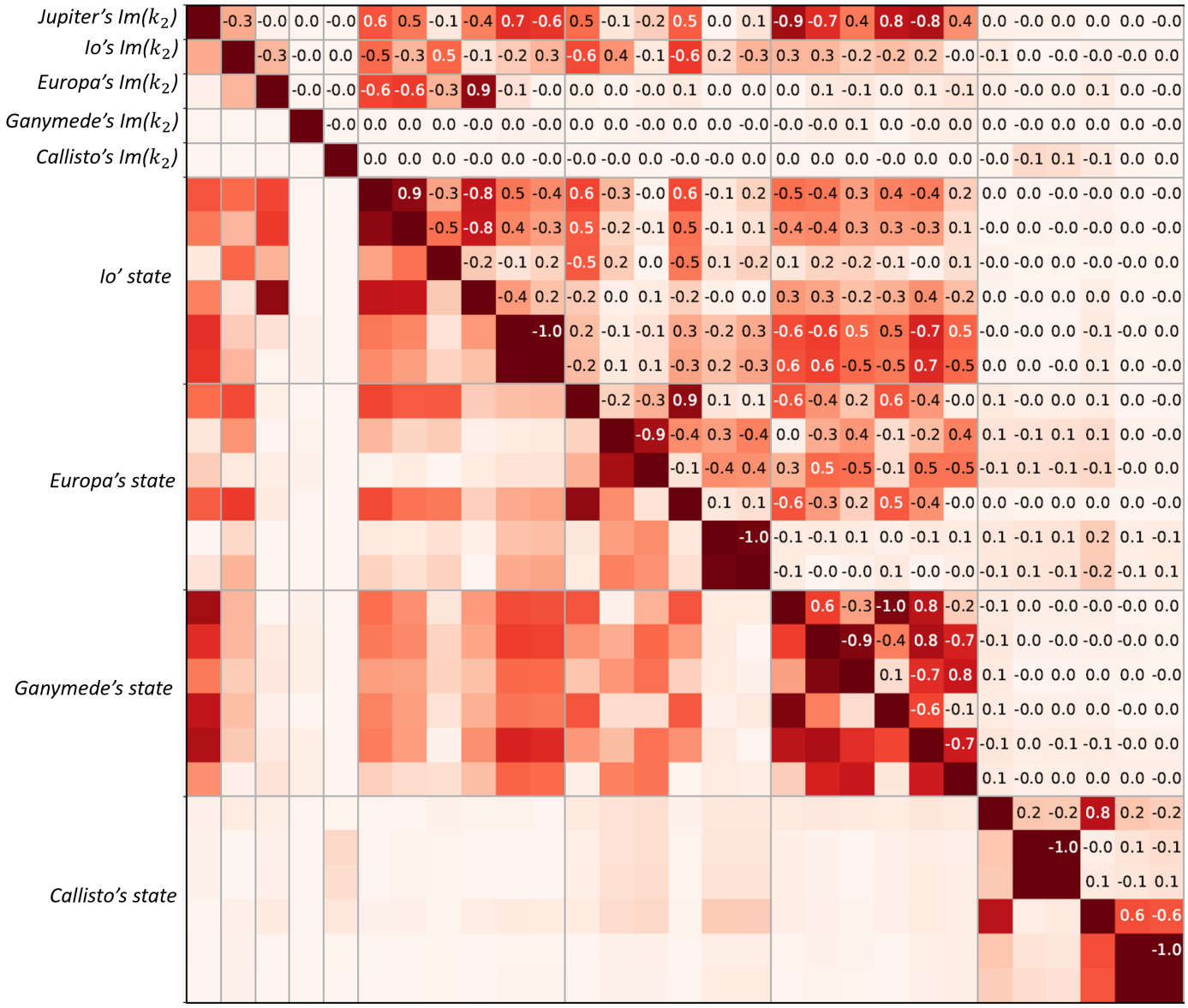

Fig. A.1. Correlation matrix for the joint solution of the dissipative parameters of Jupiter (constant Q) and the moons, and the initial states of the moons (position and velocity vectors with respect to an inertial reference frame at the reference epoch 01-JAN-2033).

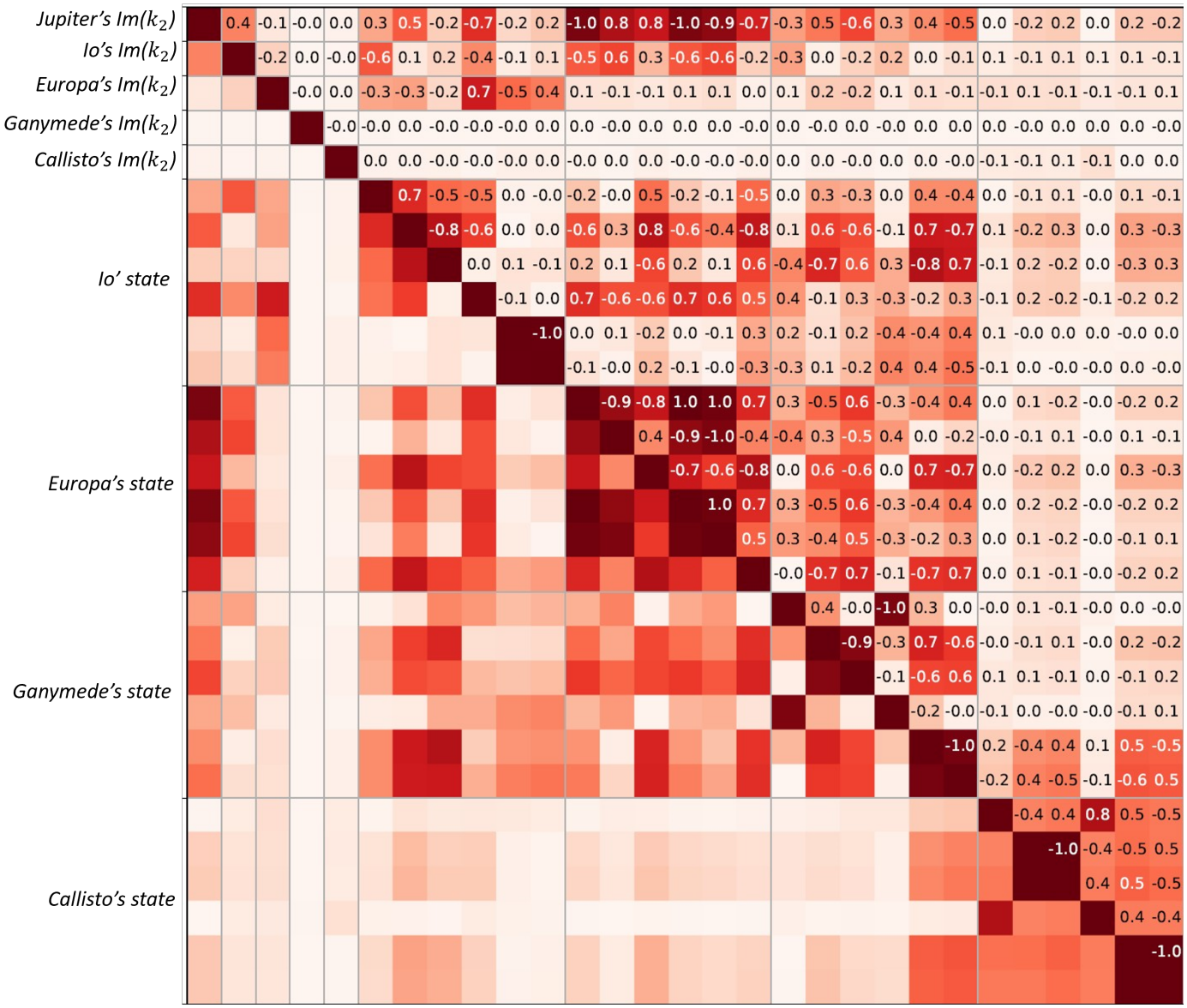

Fig. A.2. Correlation matrix for the JUICE-only solution of the dissipative parameters of Jupiter (constant Q) and the moons, and the initial states of the moons (position and velocity vectors with respect to an inertial reference frame at the reference epoch 01-JAN-2033).

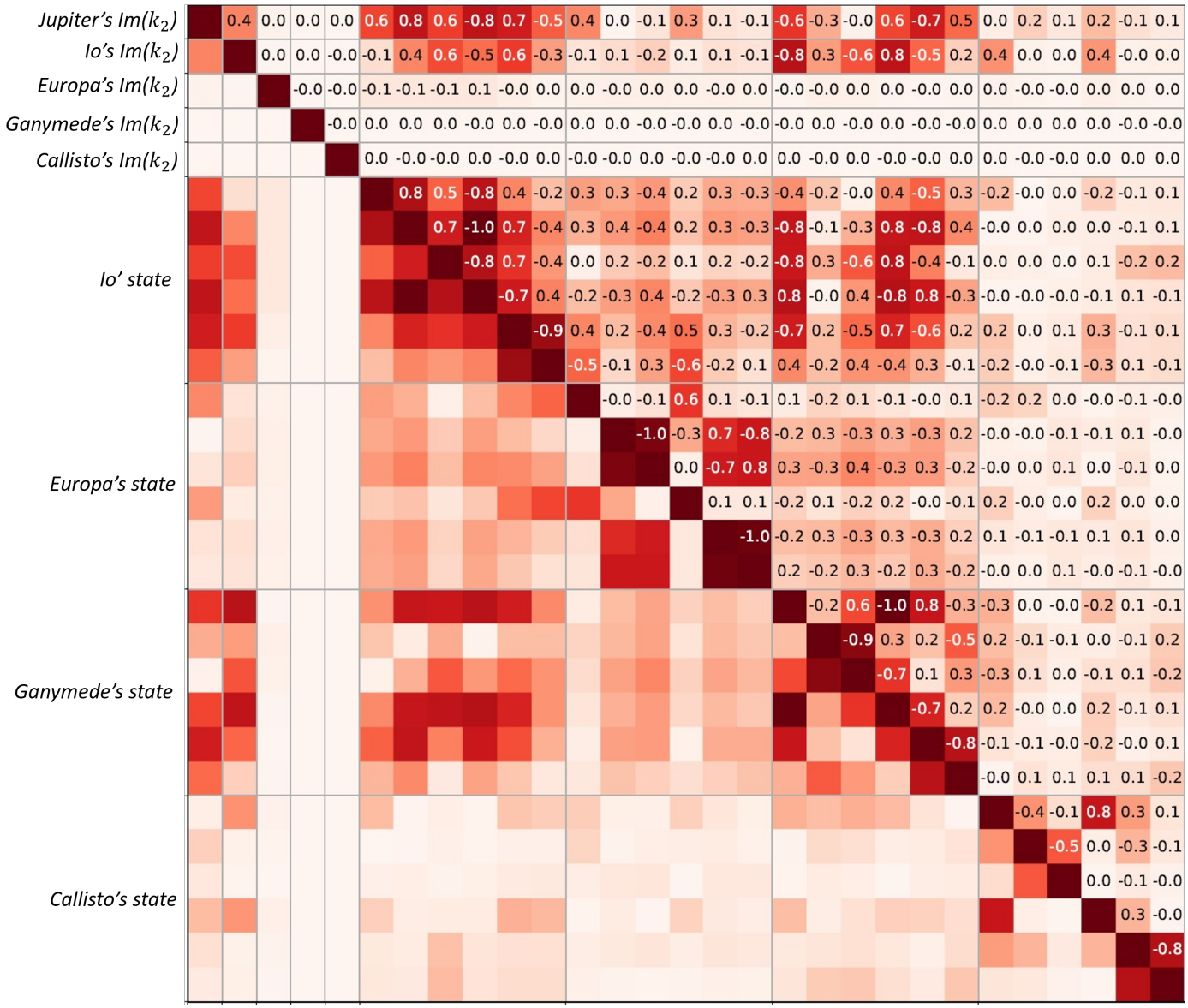

Fig. A.3. Correlation matrix for the Europa Clipper-only solution of the dissipative parameters of Jupiter (constant Q) and the moons, and the initial states of the moons (position and velocity vectors with respect to an inertial reference frame at the reference epoch 01-JAN-2033).